A MAGNETORHEOLOGICAL STUDY OF SINGLE-WALLED AND MULTI-WALLED CARBON NANOTUBE DISPERSIONS IN MINERAL OIL AND EPOXY RESIN

Zhengtao Yang, B.E.

Thesis Prepared for the Degree of

MASTER OF SCIENCE

UNIVERSITY OF NORTH TEXAS

May 2005

APPROVED:

Nandika Anne D'Souza, Major Professor
Witold Brostow, Committee Member
Rick Reidy, Committee Member
Jim Roberts, Committee Member
Jeffrey Bahr, Committee Member
Michael Kaufman, Chair of the Department of Materials Science and Engineering
Oscar N. Garcia, Dean of the College of Engineering
Sandra L. Terrell, Dean of the Robert B. Toulouse School of Graduate Studies

Yang, Zhengtao, A magnetorheological study of single-walled and multi-walled carbon nanotube dispersions in mineral oil and epoxy resin. Master of Science (Materials Science and Engineering), May 2005, 94 pp., 16 tables, 57 illustrations, references, 40 titles.

Single wall carbon nanotubes (SWNTs) and multi-walled carbon nanotubes (MWNTs) were dispersed in mineral oil and epoxy resin. The magnetorheological properties of these dispersions were studied using a parallel plate rheometer. Strain sweeps, frequency sweeps, magneto sweeps and steady shear tests were conducted in various magnetic fields. G', G", η^* and τ_y increased with increasing magnetic field, which was partially attributed to the increasing degree of the alignment of nanotubes in a stronger magnetic field. The SWNT/mo dispersions exhibited more pronounced magnetic field dependence than SWNT/ep and MWNT/mo counterparts due to their much lower viscosity. The alignment of SWNTs in mineral oil increased with rising nanotube concentration up to 2.5vol% but were significantly restricted at 6.41vol% due to nanotube flocculation.

ACKNOWLEGEMENTS

The author would like to thank Dr. Nandika Anne D'Souza for her advising. Under her guidance I learned how to use instruments, analyze data and write a paper.

I sincerely acknowledge Dr. Jeffrey Bahr at Carbon Nanotechnologies Inc. (CNI) for providing Single-walled Carbon Nanotubes for this work and his valuable advice during his two visits to our lab. The author is very grateful to Ms. Gina Paroline at Paar Physica U.S.A. Inc. for providing the magnetorheology cell and MCR 500 rheometer.

The valuable advice and suggestions by all the committee members to improve my thesis are greatly appreciated!

I would like to thank Dr. David Garrett for training me on the Transmission Electron Microscope

TABLE OF CONTENT

Page

LIST OF TABLES

Page

LIST OF ILLUSTRATIONS

Page

CHAPTER 1

BACKGROUND

1.1 Carbon Nanotubes

Since their discovery by Iijima in 1991[1], carbon nanotubes have stimulated intensive research. Numerous investigators have reported unique mechanical and physical properties of carbon nanotubes due to their structure, size and topology. A carbon nanotube (CNT) can be visualized as a single sheet of graphite rolled into a cylinder several microns in length and a few nanometers in diameter. Carbon atoms are arranged in a hexagonal array and each carbon atom has three nearest neighbors. 'Rolling' sheets of graphite into cylinders forms carbon nanotubes and often each end of a nanotube is capped. The properties of nanotubes depend on atomic arrangement (how the sheets of graphite are 'rolled'), the diameter and length of the tubes, and the morphology, or nanostructure [2].

The atomic structure of nanotubes is characterized by the tube chirality, or helicity, which is defined by the chiral vector, $\vec{C}_h$, and the chiral angle, θ. The chiral vector, often known as the roll-up vector, can be described by the following equation:

$$\vec{C} = n\vec{a}_1 + m\vec{a}_2 \tag{1.1}$$

where the integers (n, m) are the number of steps along the ziz-zag carbon bonds of the hexagonal lattice. $\vec{a}_1$ and $\vec{a}_2$ are unit vectors as shown in Fig. 1.1 [2]. The chiral angle determines the amount of 'twist' in the tube. Two limiting cases exist where the chiral angle is at 0° and 30°. These limiting cases are referred to as ziz-zag (0°) and armchair (30°) based on the geometry of the carbon bonds around the circumference of the nanotube. The difference in armchair and zig-zag nanotube structures is shown in Fig. 1.2. In terms of the roll-up vector, the ziz-zag nanotube is (n, 0) and the armchair nanotube is (n, n). The roll-up vector of the nanotube also defines the nanotube diameter since the inter-atomic spacing of the carbon atoms is known.

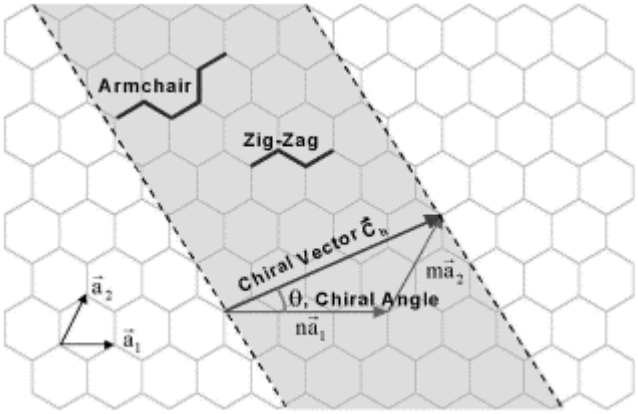

Fig. 1.1 Schematic diagram showing how a hexagonal sheet of graphite is 'rolled' to form a carbon nanotube. (Source: Figure reprinted from Composites Science and Technology with permission from Elsevier) [2].

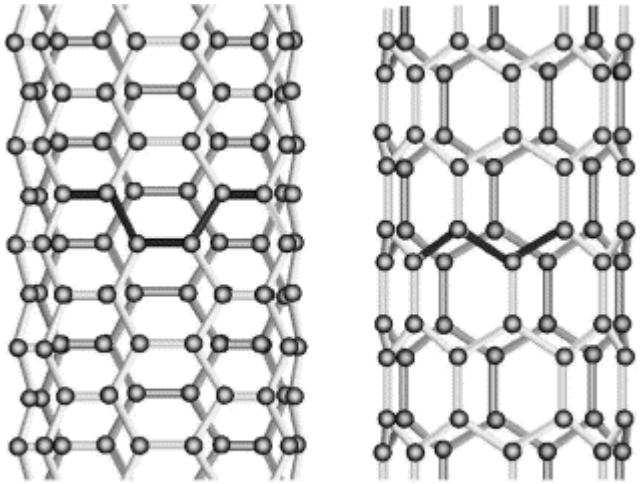

Fig. 1.2 Illustrations of the atomic structure of (a) an armchair and (b) a ziz-zag nanotube. (Source: Figure reprinted from Composites Science and Technology with permission from Elsevier) [2].

The chirality of a carbon nanotube has significant impact on the electronic and mechanical properties of carbon nanotubes. It has been shown that nanotubes can be either metallic or semiconducting depending on tube chirality [3].

Nanotubes can generally take two forms: single-walled (SWCNTs) and multi-walled (MWCNTs). Single-walled nanotubes consist of one layer of carbon atoms through the thickness of the cylindrical wall and tend to assemble as a rope consisting of 10-100 nanotubes per bundle in random tangles. Multi-walled carbon nanotubes, which were the first to be discovered, consist of concentric cylinders around a common central hollow with a constant separation between the layers held together by secondary, van der Waals bonding. Each individual cylinder has a diameter ranging from 2 to 25 nm and a length of several microns [4]. Numerous investigators have attempted to characterize carbon nanotubes

directly to better understand their mechanical properties. The measurement of SWCNT modulus has been conducted by different techniques. Treacy et al. [5] first studied the elastic modulus of isolated multi-walled nanotubes by measuring the amplitude of their intrinsic thermal vibration via transmission electron microscopy and obtained an average value of 1.8 TPa from 11 samples. Wong [6] first performed direct measurement of the elastic modulus and strength of individually isolated multi-walled nanotubes using an atomic force microscope (AFM) and obtained an elastic modulus of 1.26 TPa and a bending strength of 14.2GPa. Single-walled nanotubes often assemble as ropes of bundles. Salvetat and co-workers [7] measured the elastic and shear moduli of SWCNT ropes using AFM. They obtained an elastic and shear modulus of the order of 1 TPa and 1 GPa, respectively due to slipping of the nanotubes within the bundle. They suggested improving the intertube cohesion within SWCNT ropes. Walters [8] measured the elastic strain of freely suspended SWCNT ropes using AFM and observed an elastic strain (5.8 ± 0.9%) and a yield strength of 45 ± 7 GPa for the SWCNT ropes. Yu et al. [9] investigated SWCNT ropes and the elastic modulus ranged from 320 to 1470 GPa and the tensile strength ranged from 13 to 52 GPa. also investigated SWCNT ropes and the elastic modulus ranged from 320 to 1470 GPa and the tensile strength ranged from 13 to 52 GPa.

MWCNTs have also been investigated. Yu et al. [10] used the AFM for measuring the tensile modulus and strength of MWCNTs in the SEM. They experimentally determined tensile modulus ranged from 270 to 950 GPa and the

tensile strength ranged from 11 to 63 GPa. They observed the pull out of the inner tube after the failure of the outmost tube, a ‘sword and sheath’ telescoping failure mechanism when the MWCNT was under tensile load. In addition to their exceptional mechanical properties, nanotubes also posses superior electrical and thermal conductivities. It has been shown experimentally that the introduction of nanotubes into a polymer matrix improves the electrical conductivity of the original polymer matrix. Ultra-low electrical percolation threshold (0.0025wt%) was reported for multi-walled carbon nanotubes/epoxy composites [11]. When a three-dimensional network of filler particle through the composites is formed, that situation is known as percolation and the percolation threshold is characterized by a sharp drop in resistivity by several orders of magnitude. Nanotubes have been reported to be thermally stable up to 2800°C in vacuum and have a thermal conductivity twice as high as diamond. SWCNT/epoxy composites with only 1wt% loading showed a 125% increase in thermal conductivity [12].

The graphitic nature of the nanotube lattice results in a fiber with high stiffness, strength and conductivity. Their exceptional stiffness, strength, resilience and high aspect ratio combined with their low densities offer tremendous opportunities for the development of nanotube-based composite materials. However, SWCNTs tend to assemble in bundles (ropes) of nanotubes with weak van der Waals bonds between them and have very low solubility in most solvents. MWCNTs consist of mutiwalled co-axial tubules with weak van der Waals interactions existing between coaxial graphene layers. The main

challenges in the development of nanotube-based composites lie in the achievement of homogenous dispersion of nanotubes in the polymer matrix and strong interfacial interaction between them so as to effect efficient load transfer from the matrix to nanotubes. Due to their small size, carbon nanotubes tend to agglomerate when dispersed in a polymer matrix. To achieve effective reinforcement in a composite, it is critical to have a uniform dispersion of nanotubes in the polymer matrix. Many researchers have attempted to improve the dispersion. Gong et al. [13] used a surfactant to improve the dispersion of CNTs in an epoxy matrix, but aggregation of CNTs was still found in the matrix. Gojny et al. [14] dispersed surface modified MWCNTs in epoxy resin and observed a reduced agglomeration and improved interaction between MWCNTs and epoxy resin. Randomly oriented nanotube-polymer composites have been investigated extensively in terms of their mechanical and electrical properties. Due to the high aspect ratio of nanotubes, a high anisotropy is expected for nanotube-polymer composites therefore orientation of nanotubes greatly influences nanocomposite properties. To utilize the anisotropic nature of nanotubes, make the best use of their axial exceptional high stiffness and strength, and realize increased mechanical properties in nanocomposites, it is important to control the alignment of nanotubes in a polymer matrix. Several groups have achieved the alignment of nanotubes in a polymer matrix. Ajayan et al. [15] randomly dispersed nanotubes in epoxy matrix. Slicing the composite resulted in partial alignment of the nanotubes on the cut surface. Jin [16]

fabricated polymer-based composites with aligned MWCNTs by casting a suspension of nanotubes in a solution of a thermoplastic polymer and chloroform and uniaxially stretching the composites at 100°C. The degree of alignment can be controlled by controlling the stretching ratio. Thostenson [17] dispersed MWCNTs in a polystyrene matrix using a micro-scale twin-screw extruder and produced highly aligned composite films by extruding the composite melt through a rectangular die and drawing the film prior cooling. They found improvement in the elastic modulus in the aligned nanotube composite was 5 times greater than the improvement in a randomly oriented composite.

A high magnetic field is a direct and efficient means to align nanotubes. A magnetic field has been found to have strong effects on the electronic and bulk properties of nanotubes. Ramirez and coworkers [18] have found nanotubes have significantly larger orientation-averaged susceptibility, on a per carbon basis, than any other form of elemental carbon. Lu [19] has predicted a field-induced metal-insulator transition for all nanotubes. The magnetic susceptibility was predicted to be large and increase linearly with the nanotube radius. The susceptibility can be either diamagnetic or paramagnetic in a weak field depending on the field direction, the Fermi energy, the helicity of the nanotubes, and the nanotube radius. Nanotubes have been predicted to have an anisotropic magnetic susceptibility. Wang [20] measured the magnetic susceptibility of buckybundles parallel and perpendicular to the bundle axes and found the buckytubes had anisotropic diamagnetic properties. The lowest energy

orientation of nanotubes is parallel to the field so a strong magnetic field can align nanotubes in a liquid suspension. This is similar to the alignment of liquid crystals in a magnetic field. The magnetic orientation of nanotubes is explained by the susceptibility anisotropy [21]. They are magnetically symmetric along the tube axis and have molar susceptibilities parallel ($\chi_{\parallel}$) and perpendicular ($\chi_{\perp}$) to it. The magnetic energy of nanotubes composed of mole number n of carbon atoms in a field H is given by

$$E(\theta, H) = -(nH^2/2)[\chi_{\perp} + (\chi_{\parallel} - \chi_{\perp})\cos^2\theta] \quad (1.2)$$

Where θ is the angle between the tube axis and field H. The orientation of nanotubes in a magnetic field occurs so that the energy E (θ, H) is a minimum. Experimental observations showed nanotubes were aligned with the tube axis parallel to the field (θ = 0). Nanotubes are considered to be diamagnetic at 310 K, that requires the condition of $\chi_{\perp} < \chi_{\parallel} < 0$. The field intensity dependence of the orientation of nanotubes is interpreted as the Boltzmann distribution for the directions of different magnetic energy [21]. The magnetic energy is a minimum and nanotubes are stable when the nanotube axis is parallel to the field (θ = 0). If the magnetic field strength is low, the difference in magnetic energy is small between the stable direction (θ = 0) and any direction and the orientation is disordered by the thermal energy. When the magnetic field strength increases, the difference in magnetic energy is larger and the probability of orientation in the stable direction becomes higher. Fujiwara [22] suspended MWCNTs in carbon tetrachloride and placed them in magnetic fields of around 80.0 kOe at 310 K.

They found that a single and free nanotube is oriented with the tube axis parallel to the fields using SEM and estimated the anisotropy of susceptibilities parallel ($\chi_{||}$) and perpendicular ($\chi_{\perp}$) to the tube axis to be $\chi_{||} - \chi_{\perp} \sim (9 \pm 5) \times 10^{-6}$ emu per mole of carbon atoms ($\chi_{\perp} < \chi_{||} < 0$). Calculations have shown that metallic SWCNTs are paramagnetic in the direction of their long axes and tend to align parallel to an external magnetic field. Some SWCNTs are diamagnetic and their diamagnetic susceptibilities are most negative in the direction perpendicular to the tube axis, causing them to align parallel to the direction of an external magnetic field. The alignment energies for both magnetic and diamagnetic SWCNTs are comparable. The predicted molar susceptibility for a (10, 10) nanotube are: $\chi_{||}^{m} = +85.4 \times 10^{-6}$ emu $(\text{molC})^{-1}$when parallel to B, and $\chi_{\perp}^{m} = -21.0 \times 10^{-6}$ emu $(\text{molC})^{-1}$ when perpendicular. The alignment energy is small and the effects of thermal energy should be considered. The potential energy U of a nanotube containing *n* moles of carbon is $U(\theta) = -B^2 n(\chi_{||}^{m} \cos^2\theta + \chi_{\perp}^{m} \sin^2\theta)$, where θ is the angle between the nanotube axis and the magnetic field. Each nanotube undergoes Brownian motion in this potential with an average energy of $k_B T$, where T is room temperature. The alignment energy is $\Delta U = U(\pi/2) - U(0) = B^2 n(\chi_{||}^{m} - \chi_{\perp}^{m})$. ΔU must be many times $k_B T$ in order to obtain good alignment of nanotubes. For a (10, 10) nanotube of length 300 nm, a field of 15.3 T gives $\Delta U = 5\ k_B T$ [23]. The alignment energy is proportional to the number of moles of carbon. A bundle of nanotubes requires a lower magnetic field to achieve alignment than an individual nanotube with the same length [23].

Walters et al. [23] have produced highly aligned SWCNTs in thin membranes by introducing a suspension of SWCNT segments to a strong magnetic field to align the segments and filtering the suspension in the magnetic field. The resulting membranes displayed natural cleavage planes parallel to the magnetic field. Casavant et al. [24] have fabricated thick macroscopic membranes of aligned SWCNTs via high-pressure filtration of aqueous surfactant-suspended nanotubes using magnetic field strengths of 7 and 25 T. Their 10μm-thick membrane with surface areas of 125 cm showed anisotropy of (2.5±0.5) via polarized Raman spectroscopy. Kimura [25] prepared an anisotropic MWCNT/polyester composites using a high magnetic field of 10 T. MWCNTs were found to be aligned parallel to the magnetic field inside the polymer matrix. Results of magnetic susceptibility, electric conductivity, and elastic modulus measurements showed clear anisotropy.

1.2 Rheology

1.2.1 Definition of rheology and its importance

Rheology can be defined as the science of the flow and deformation of matter. It deals with the fundamental relations between force and deformation in materials, primarily liquids. For low-molecular-weight fluids, rheology involves the measurement of viscosity. For such fluids, viscosity depends primarily on the temperature and hydrostatic pressure. The rheology of high-molecular-weight liquids such as polymer liquids, whether neat or filled, is much more complex because polymer fluids show nonideal behavior. Polymer liquids show complex

shear viscosity and elastic properties. All these rheological properties depend upon the rate of deformation, the molecular weight and structure of polymer, and the concentration of various fillers, as well as the temperature [26].

The subject of rheology is very important for polymers and polymer composites. There are two main reasons. First, flow is involved in the processing of polymers and composites to fabricate useful objects. So fluid rheology is closely related to polymer processing and determines stress levels in operation such as extrusion and fiber spinning. Similarly, rheology influences residual stresses, cycle times, and void content in composite processing operations such as compression molding and injection molding. Therefore, a quantitative description of polymer and composite rheology is essential for developing models of various polymer processing operations. These models can be used for process optimization and for predicting the onset of flow instabilities. Second, mechanical properties of polymers are extremely important and are influenced by rhelological behavior. For example, molecular orientation has significant effects on the mechanical properties of molded products, fibers and films. For short-fiber composites, fiber orientation plays the role of molecular orientation in unfilled systems. The degree of molecular or fiber orientation are largely determined by the rheological behavior of the polymer and the nature of the flow in the fabrication process [26].

1.2.2 Materials Functions in Viscometric Flows

The flow field that is generated in most standard instruments used to

measure rheological properties is a shear flow called viscometric flow. All the motion in a viscometric flow is along one coordinate direction x_1 and the velocity varies along a second coordinate x_2 and the third direction is neutral. If a liquid is confined between two flat plates of area A separated by a distance D. When the upper plate moves in the x_1 direction relative to the lower plate, the liquid is sheared with the amount of shear strain γ being defined as

$$\gamma = \frac{S}{D} \tag{1.3}$$

Where S is the amount of shear displacement and D is the distance between shear surfaces.

The rate of shear strain is defined as

$$\dot{\gamma} = \frac{d}{dt}\left(\frac{S}{D}\right) \tag{1.4}$$

The rate of shear strain is often referred to as the shear rate. A force is needed to move the top plate at a constant velocity relative to the lower plate. This is the shear force and one gets the shear stress τ when the shear force is divided by the area of the shear face. For a Newtonian liquid, the shear stress is directly proportional to shear rate and the proportionality is called the dynamic viscosity η. The relationship is shown below

$$\tau = \eta \dot{\gamma} \tag{1.5}$$

If the liquid is not Newtonian, a plot of τ-versus-$\dot{\gamma}$ is a curve. Generally, the shear viscosity of polymers decreases with increasing shear rate. This behavior is shear thinning. If the relative velocity of the shear plates varies in a sinusoidal

manner so that both shear strain and shear rate are cyclic, the shear stress is also sinusoidal. A dynamic mechanical experiment is one in which a polymer is subjected to a sinusoidal strain γ of infinitesimal amplitude γ_0 and fixed angular frequency ω;

$$\gamma = \gamma_0 \sin \omega t \tag{1.6}$$

The stress response τ is also sinusoidal but, in general, is out of phase by an angle δ.

$$\tau = \tau_0 \sin (\omega t + \delta) \text{ or } \tau = (\tau_0 \cos \delta) \sin \omega t + (\tau_0 \sin \delta) \cos \omega t \tag{1.7}$$

On dividing the stress by the strain amplitude, we get the complex modulus, G^*:

$$G^* = G'(\omega) \sin \omega t + iG''(\omega) \cos \omega t \tag{1.8}$$

Where $G' = (\tau_0 \cos \delta)/\gamma_0$ and $G'' = (\tau_0 \sin \delta)/\gamma_0$. G' is the storage modulus or dynamic rigidity and is defined as the component of the stress in phase with the strain divided by the strain amplitude and represents the energy stored and recovered per cycle. The loss modulus, G", is defined as the stress component out of phase with the strain divided by the strain amplitude and represents the energy dissipated as heat per cycle of deformation. The ratio of G"/G', $\tan \delta$, is a measure of energy dissipation in viscoelastic materials. For a perfectly elastic material, G" is zero while for a Newtonian liquid that is perfectly viscous, G' is zero. Generally, both G' and G" are functions of frequency. In these dynamic mechanical experiments, there exist two extreme cases. For a perfectly elastic material, the shear stress and shear strain are in phase. For a perfectly viscous material, the strain rate, $d\gamma/dt$, responds linearly to the shear stress with a

proportionality constant η and the strain lags the stress by 90°. The general case of a viscoelastic material will result in a displacement between the two extremes. That is, the strain will lag the stress by between 0° and 90° and the angle separating τ and γ is the loss angle δ. In this situation, a complex viscosity, η^*, can be measured. The complex viscosity is defined as:

$$\eta^* = \frac{G^*}{i\omega} = \frac{G'+iG''}{i\omega} = \frac{G''}{\omega} - \frac{iG'}{\omega} = \eta' - i\eta'' \qquad (1.9)$$

The dynamic viscosity η' is related to the steady state viscosity and is the part of the complex viscosity that measures the rate of energy dissipation . The imaginary viscosity, η'', measures the elasticity or stored energy. These two viscosities are calculated from the real and imaginary parts of the shear modulus G^* by the following relations:

$$\eta' = \frac{G''}{\omega} \qquad (1.10)$$

$$\eta'' = \frac{G'}{\omega} \qquad (1.11)$$

where ω is the frequency of the oscillations in radians per second.

1.3 Rheology of Filled Systems

The rheology of suspensions containing rigid fillers is very important in many systems. Composites containing filler weight fractions in the range of 0.4-0.65 are common, and the fillers act either as reinforcements or as diluents. Fillers have a profound effect on the rhelogical behavior of the suspension.

Einstein [27] first predicted the effect of a rigid filler on the viscosity of a Newtonian liquid. His equation for the flow of dilute suspensions is

$$\eta = \eta_0 (1 + k_E \varphi) \qquad (1.12)$$

Where η is the viscosity of the mixture, η_0 is the viscosity of the suspending liquid, φ is the volume fraction of filler and k_E is the Einstein coefficient. For particles of spherical shape, k_E is 2.5. The magnitude of k_E is determined by the degree to which the particles disturb the streamlines in a flowing system. Some particle shapes, such as rods, disturb the streamlines more than spheres do and have larger Einstein coefficients. For uniaxially oriented fibers parallel to the the tensile stress component, the Einstein coefficient is 2L / D, where L / D is the fiber aspect ratio. The Einstein equation is valid only for very low concentrations of particles (< 1%).

Most polymer liquids are non-Newtonian and display shear thinning. The addition of the same amount of particulates raises the viscosity more at low shear rates than at higher shear rates. Therefore, the relative viscosity depends on the shear rate as well as on the filler concentration. The addition of fillers to a polymer fluid results in an increase in the storage and loss moduli at a given frequency.

When fine particles are dispersed in low-viscosity liquids, the rheological behavior is the result of interplay between hydrodynamic, van der Waals, coulombic and Brownian motion forces. For concentrated systems, Brownian motion is relatively weak and the rest state is characterized by the formation of

flocs. The formation of flocs is the result of particle-particle interactions due to surface forces. When suspensions are prepared in organic or nonpolar media, coulombic effects are unimportant and the van der Waals forces of attraction between suspended particles cause flocculation, trapping liquid and forming a gel. This results in a high viscosity and the appearance of an apparent yield stress with decreasing shear rate. The floc sizes can be reduced by shearing and severe shear shinning is observed. If shearing is stopped, the structure can reform. If the time scale for recovery is large, time-dependent effects or thixotropy can occur.

The rheological behavior of nanotube dispersions has been investigated. Shaffer [28] found aqueous dispersions of carbon nanotubes had two different concentration regimes: Dilute dispersions exhibited polymer solution behavior such as an entanglement-like transition and a viscoelastic gel was formed for nanotube concentrations above 5 vol%. Kinloch et al. [29] studied the rheological behavior of concentrated aqueous nanotube dispersions above 0.5 vol%, and observed reversible flocculated dispersions wherein G' and G" scaled with concentration by a power law independent of frequency. Pötschke [30] investigated the rheological behavior of multi-walled carbon nanotube/polycarbonate composites containing between 0.5 and 15wt% carbon nanotubes using oscillatory rheometry at 260°C. The viscosity increase associated with the addition of nanotubes was much higher than the viscosity increase for carbon nanofibers and carbon black composites due to the higher

aspect ratio of the nanotubes. Composites with more than 2wt% nanotubes exhibited non-Newtonian behavior at lower frequencies. They also observed a step increase at 2 wt% nanotubes in the viscosity-composition curves at low frequency and regarded this step change as a rheological threshold, which coincided with the electric conductivity percolation threshold.

1.4 Magnetorheology

Magnetorheological (MR) fluids consist of meso-scale (1-10um) ferromagnetic or ferromagnetic particles with high permeability dispersed in a viscous or viscoelastic nonmagnetizable liquid. The most common magnetic material used for the preparation of MR fluids is high purity iron powder derived from decomposition of iron penta-carbonyl ($Fe(CO)_5$). In the absence of an applied magnetic field, (MR) fluids typically behave as nearly ideal Newtonian liquids. The application of a magnetic field induces a magnetic dipole and multipole moments on each particle. The anisotropic magnetic forces between pairs of particles promote the head-to-tail alignment of the moments and draw the particles into proximity. These attractive interparticle forces result in the formation of chains, columns, or more complicated networks of particles aligned with the direction of the magnetic field. Magnetic flux density of the order of 0.1 Tesla can greatly increase the viscosity of MR fluids by several orders of magnitude. When these structures are deformed mechanically, magnetic restoring forces tend to oppose the deformation [31]. Their flow in an external magnetic field undergoes a competition between magnetic and hydrodynamic

forces. This competition gives rise to the original rheological properties with the creation of an apparent yield stress and a rapid and reversible liquid-solid transition. Rabinow first reported the MR effect in 1948 [32]. MR fluids can exhibit yield stress of the order of 100 kPa, two orders of magnitude larger than electrorheological (ER) fluids, when they are exposed to magnetic fields of 240 kA/m. The availability of MR fluids with yield stresses that are controllable over many orders of magnitude by applied fields enables the construction of electromechanical devices that are controlled by electrical signals. The substantial field-induced yield stresses exhibited by MR fluids result in its use in rotary couplings. Rotary brakes and linear dampers utilizing MR fluids are in commercial production. Many ceramic, metal and alloy based compositions have been described and can be used to prepare MR fluids. Particles used are magnetically multi domain and exhibit low levels of magnetic coercivity. Ginder [33] investigated MR fluids using numerical and analytical models and identified three regimes: at low applied fields, the yield stress increases with applied field H_0 as $\tau_y \sim H_0^{3/2}$. In intermediate fields, the contact or polar regions of each particle saturate, reducing the rate of increase of the stress with increasing field. At high fields, the particles saturate completely, and the stress reaches its limiting value. Klingenberg [40] examined the flow modification in MR fluids associated with the field-induced magnetization of the dispersed phase relative to the continuous phase. At moderate to high particle concentration, the structure mainly consists

of thick clusters. The relaxation process is related to a frequency dependent dynamic structure within the cluster.

CHAPTER 2

EXPERIMENTAL PROCEDURES

2.1 Materials

Purified Single Wall Carbon Nanotubes (SWCNTs) were provided by Carbon Nanotechnologies Incorpatated (CNI) in Houston with a density of 1.4 g cm^{-3}. Multi-walled Carbon Nanotubes (MWCNTs) were provided by Mitsui in Japan with a density of 1.75 g cm^{-3}. Transmission electron microscopy (TEM) was used to characterize the morphology of the nanotubes using the following procedure. 6 mg of nanotubes were placed in 100 ml of 5% nitric acid HNO_3 for 24 hours to dissolve the metal residual such as iron nanoparticles. 1 mg of nanotubes was dispersed in 20 ml of ethanol in a glass beaker and the dilute suspension was ultrasonicated for 30 minutes to disentangle the nanotubes. Several drops of the suspension were added to the copper grid and examined by transmission electron microscopy (TEM) operated at an accelerating voltage of 100kV. The TEM micrographs of SWCNTs are shown in Fig. 2.1 and Fig. 2.2. The SWCNTs are still in ropes after ultrasonic vibration and the rope diameter is about 200 nm.

Fig. 2.1 A TEM micrograph of SWCNTs at a low magnification.

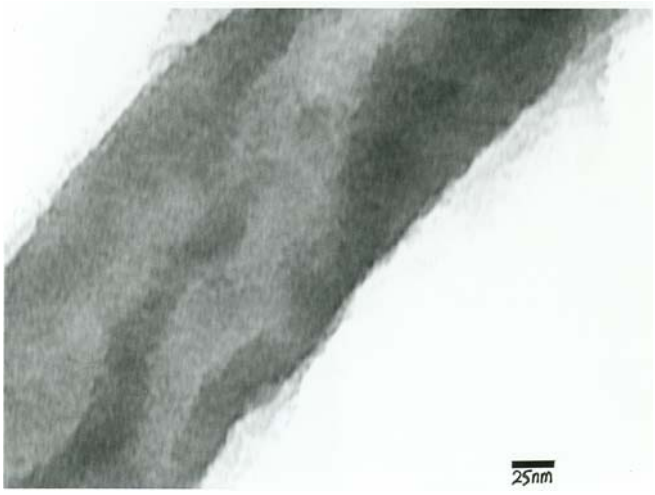

Fig. 2.2 A TEM micrograph of SWCNTs at a high magnification.

A TEM micrograph of a MWCNT is shown in Fig.2.3. The length of the nanotube is beyond the edge of the image revealing its high aspect ratio. The diameter of the MWCNT is around 200 nm.

Fig. 2.3 A TEM micrograph of a MWCNT at a low magnification

The iron contents of SWCNTs and MWCNTs were determined to be 1.04wt% and 0.281wt%, respectively by atomic absorption. 6.2 mg of nanotubes were dissolved in 100 ml of 5% nitric acid HNO_3 solution in a flask for 24 hours. Mineral oil was purchased from Roberts Pharmaceutical Corporation. Roberts Mineral oil is a hydrocarbon oil with a density of 0.863 g cm^{-3}. It contains dl-tocopherol as a preservative. It has a very low shear viscosity of 0.42 Pa.s at 25°C and nanotubes can easily rotate and align along the field direction in this medium. Mineral oil is a nonmagnetic isolating fluid and is often used as a base fluid for making conventional MR fluids besides silicone oils [34], [35]. The epoxy resin EPON 828 was purchased from Miller-stephenson Chemical Company, Inc. and was a liquid diglycidyl ether of bisphenol A-based (DGEBA) epoxy resin with a density of 1.17 g cm^{-3}. Epoxy systems are very important and have been widely used in aircraft, electronics and many other industrial applications and are

typical matrices for fabricating composites. Investigation of the alignment of CNTs in epoxy resin in a magnetic field should have practical significance.

2wt%, 4wt% and 10wt% SWCNTs were dispersed in mineral oil and the corresponding volume fractions of nanotubes were 1.24vol%, 2.5vol% and 6.41vol% respectively. 2wt% and 4wt% SWCNTs were dispersed in epoxy resin and the corresponding volume fractions of nanotubes were 1.68vol% and 3.37vol%. 1wt%, 3wt% and 5wt% MWCNTs were dispersed in mineral oil and the corresponding volume fractions of nanotubes were 0.5, 1.5 and 2.53vol% respectively. 1wt% and 3wt% MWCNTs were dispersed in epoxy resin and the volume fractions of MWCNTs are 0.67% and 2%, respectively.

To prepare the dispersion, nanotubes were added to mineral oil or epoxy resin in a glass beaker and the mixture was stirred manually by hand for about 2 minutes and heated in oven at 50°C for about 3 minutes to reduce the viscosity. The dispersion was mixed again until it cooled down. The same procedure was repeated three times to get a uniform dispersion.

2.2 Instrument and Magnetic Field setup

A Physica rheometer MCR 500 provided by Parr Physica was used for rheological investigation of the dispersions. A picture of the instrument is shown in Fig.2.4 and a schematic of magnetic setup is shown in Fig.2.5. There are two parameters that impact the quality of rheological measurements, namely, torque and displacement. For the rheometer MCR 500, the torque precision has a maximum of 0.2 (μNm) and 0.5% of the actual torque. At low torques, the first

criterion will dominate. At higher torques, the percentage will take over. The displacement precision is better than 1% within the range of instrument specifications.

Applying an electric current to a coil below the bottom plate produces a magnetic field perpendicular to the parallel plates. The coil current and the magnetic field strength are variably controlled by a separate control unit and rheometer software. The control unit automatically demagnetizes the system upon completion of the experiment. A parallel-plate measuring system with a diameter of 20 mm was used. The measuring system is made of non-magnetic metal to prevent radial magnetic forces from acting on the shaft of the measuring system. A two-part cover served as a magnetic bridge and gave a uniform magnetic field. The measuring system was PP 20/MR and the selected gap was 0.5 mm. The required sample volume for each measurement was 0.4 cm^3 and a syringe of 1 cm^3 was used to load 0.4 cm^3 of the dispersion onto the lower plate. The plate temperature was kept at 25°C during test using a water circulator.

Fig. 2.4 A Picture showing the Physica rheometer MCR 500 [36].

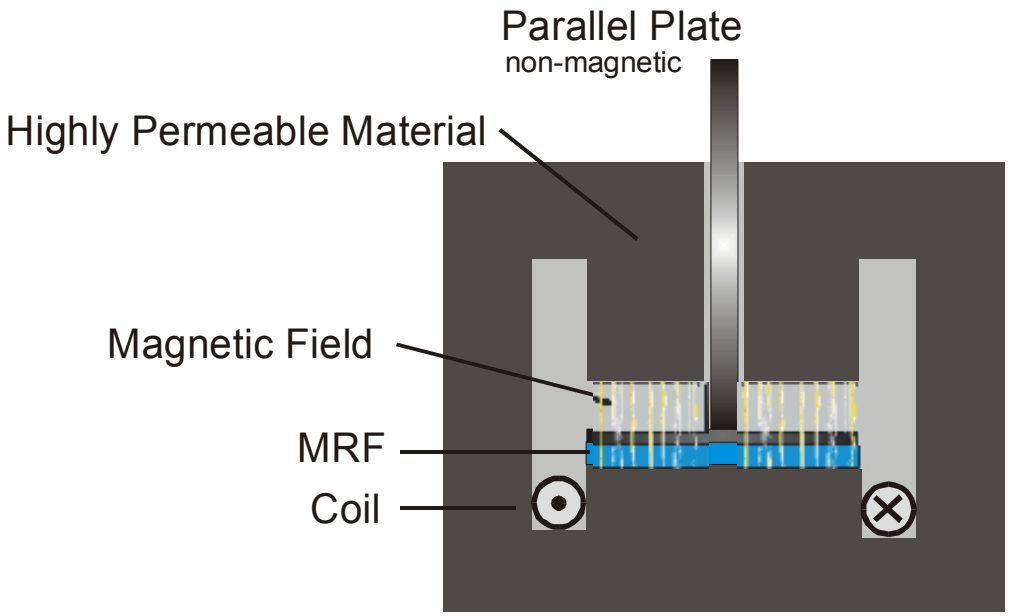

Fig. 2.5 A schematic of test setup for producing magnetic field in MCR 500 [36].

3.3 Magnetorheological tests

Oscillatory tests at sufficiently low deformations were carried out to avoid destroying the structure of dispersion. The desired constant magnetic field was applied to the dispersion for 1 minute without shear prior to initiating the rheological measurements under the same field. First, the linear viscoelastic region (LVR) was determined by dynamic strain sweeps at a constant frequency of 1 Hz under different magnetic fields. G', G" and τ were recorded. Second, dynamic frequency sweeps were conducted at a constant strain of 0.4% within the LVR under different magnetic fields to investigate the structure of the dispersions. In these sweeps, the angular frequency ω was ramped logarithmically from 100 to1 (rad/s) with 6 data points collected in each decade.

G', G" and damping factor, tan δ were measured. Third, steady shear tests were conducted to investigate the flow behavior of the dispersions and flow curves were obtained with a controlled shear rate (CSR) under different magnetic fields. $\dot{\gamma}$ was ramped logarithmically from 10 to 1000 (1/s) for SWCNT/mo dispersions and from 0.1 to 100 (1/s) for SWCNT/ep dispersions with 6 data points collected in each decade. For MWCNT/mo dispersions, $\dot{\gamma}$ ramped logarithmically from 10 to 200 (1/s). The flow data were fitted to the Bingham model [37]. This model is widely used for suspensions, paint and food substances etc. which are called viscoplastic or Bingham plastics after E.C. Bingham, who first described paint in this way in 1916. A Bingham plastic shows little or no deformation up to a certain level of stress called a yield stress. Above the yield stress the material flows readily like a Newtonian fluid. In shearing flows, the steady-state rheological response of MR fluids is usually modeled as a Bingham fluid, with a magnetic field-dependent dynamic yield stress $\tau_y(B)$,

$$\dot{\gamma}=0 \qquad \text{for } \tau < \tau_y$$

$$\tau(B) = \eta\dot{\gamma} + \tau_y(B), \quad \text{for } \tau \geq \tau_y \tag{2.1}$$

Where τ is the shear stress. $\dot{\gamma}$, τ_y and η are the shear rate, dynamic yield stress and viscosity, respectively.

A magneto- sweep is an oscillatory test method with constant strain amplitude and constant frequency while the magnetic field strength is increased either logarithmically or linearly. In contrast to the flow curve from a steady shear

test, a magneto sweep allows accurate determination of a magnetorheological fluid's viscoelastic properties as a function of the preset magnetic field strength [35] In our magneto sweeps, the strain was kept constant within the LVR at a constant frequency of 1 (rad/s) while the magnetic field strength was linearly ramped from zero to 343kA/m.

CHAPTER 3

RESULTS AND DISCUSSION

Pure mineral oil and epoxy resin were first tested to determine its response to the magnetic field. Strain sweeps, frequency sweeps, steady shear tests in various magnetic fields and magneto sweeps for mineral oil showed that G', G" and η^* remain approximately the same in different magnetic fields. All results are therefore reported for the nanotubes/mineral oil and nanotubes/epoxy resin dispersions.

3.1 Single-walled Carbon Nanotube/Mineral Oil Dispersions

3.1.1 Strain Sweeps of SWCNT/mo Dispersions

The results of strain sweeps for 1.24vol%, 2.5vol% and 6.41vol% SWCNT/mo dispersions are shown in Fig. 3.1, Fig. 3.2 and Fig. 3.3, respectively. The values of G' at a strain of 1% for these compositions under different fields are tabulated in Table 3.1. Under the same magnetic field, G' increases significantly with increasing nanotube concentration. Also of note, for a given composition, G', G" and τ increase with increasing magnetic field strength. For instance, the values of the G' show increases of 2119 % for 1.24 vol% SWCNT/mo and 3532 % for 2.5 vol% for an applied field strength of 343 kA/m, relative to the case of no applied field. These results indicate that the alignment of the nanotubes restricts the motion of the base fluid in the flow direction, and

leads to increases in complex shear moduli, as indicated by the field strength dependence, in a concentration dependent manner. For the 6.41 vol% SWCNT/mo composition, however, the relative increase in G' is only 1241 %. This fact alone indicates that the residual iron content of the SWCNT is not the main reason for the observed increases G' with field strength. The response of the 6.41vol% suspension can be interpreted as a truly flocculated suspension, wherein the nanotube concentration is sufficient to inhibit rotation and alignment of the nanotubes along the field direction, resulting in a smaller increase in modulus compared to lower concentrations. For the 1.24vol% and 2.5vol% compositions, linear viscoelastic behavior is evident at low strains (up to 1%), and the LVR is extended with increasing field strength. Again, for the 6.41vol% composition, this is not observed. The shear stress increases roughly linearly with strain without applied field, indicating linear viscoelastic behavior. When a constant magnetic field is applied, however, two distinct regimes are observed for the dispersions with low nanotube concentrations. As shown in Figure 3.1b, the linearity between τ and γ disappears in the low strain regime and the slope of τ vs. γ gradually decreases with increasing strain up to a strain of 20 % in regime 1 and then become roughly constant with larger strain in regime 2. For even higher nanotube concentration such as 6.41vol%, as shown in Figure 3.3b, four regimes are evident. Under a magnetic field of 343kA/m, for example, the slope first decreases continuously up to the strain of 12% in regime 1 and then becomes constant until the strain of 48% in regime 2. The slope increases abruptly and

become constant up to the strain of 68% in regime 3. After the strain of 68%, the slope increases suddenly and becomes constant in regime 4. Increasing strain amplitude helps SWCNT ropes to be aligned along the field direction and make the ropes stiffer. When a small strain is applied to the dispersion, a G' and G" crossover, implying a solid-liquid transition, is evident for the 6.41vol% composition. A critical strain, $\gamma_{c,}$ is defined as the strain at which G' and G" are equal and represents the transition between viscoeleastic solid (low strain) to viscoelastic fluid (high strain). When there is no field applied, this crossover is not observed for the 6.41vol% composition. However, critical strains of 0.683% and 1.135% occur under applied field strengths of 171kA/m and 343kA/m, respectively, indicating γ_c increases with increasing magnetic field. This parameter is related to the dispersion and reflects the competition between magnetic forces and hydrodynamic forces. In the present 6.41vol% composition, this transition is reflective of the presence of a flocculated network.

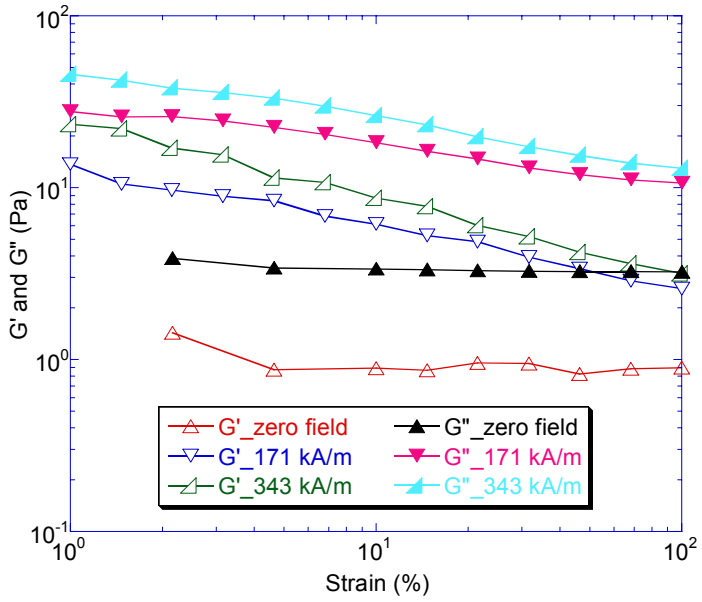

(a)

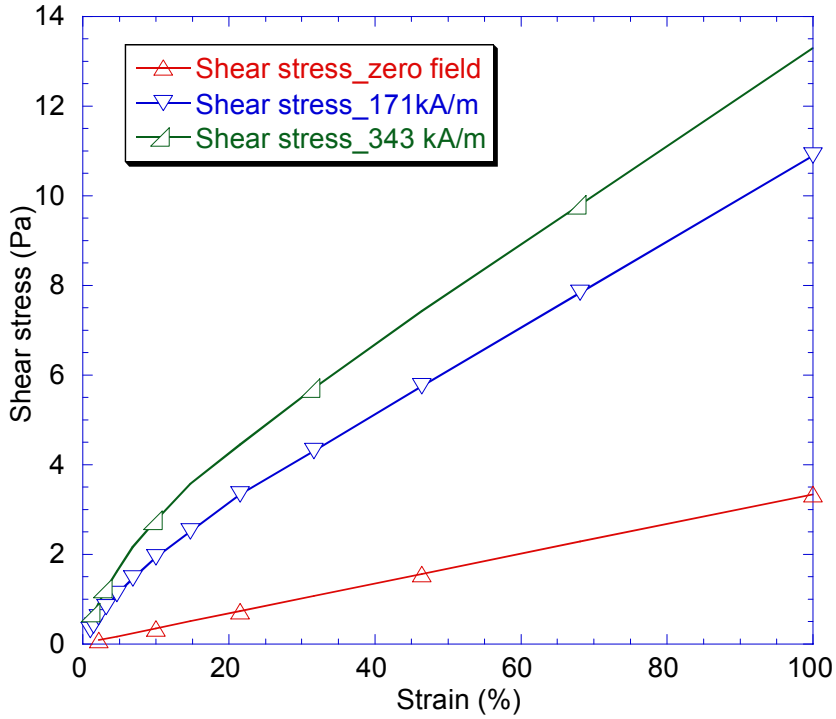

(b)

Fig. 3.1 Strain sweeps for 1.24vol% SWCNT/mo dispersions showing (a) increase in G' and G", and (b) increase in τ with increasing magnetic field.

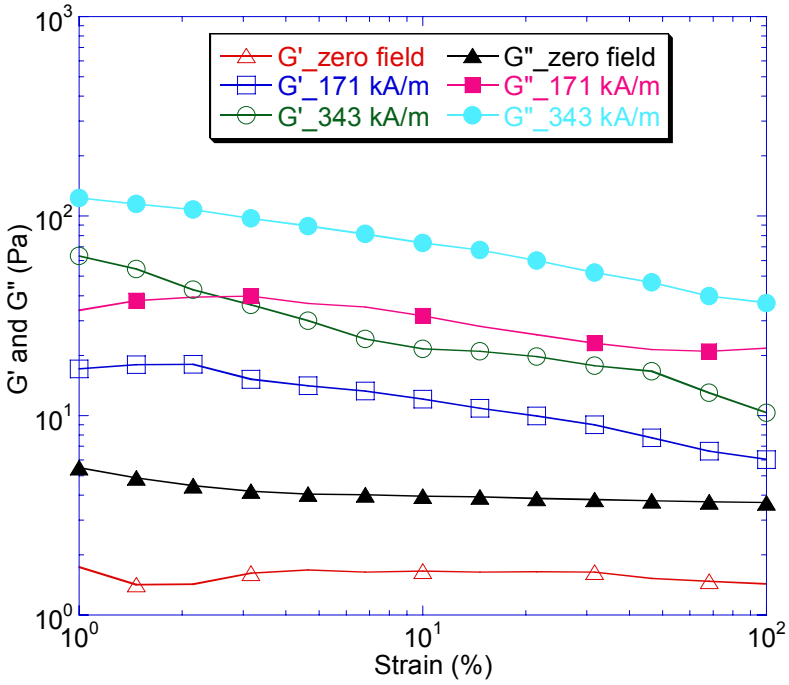

(a)

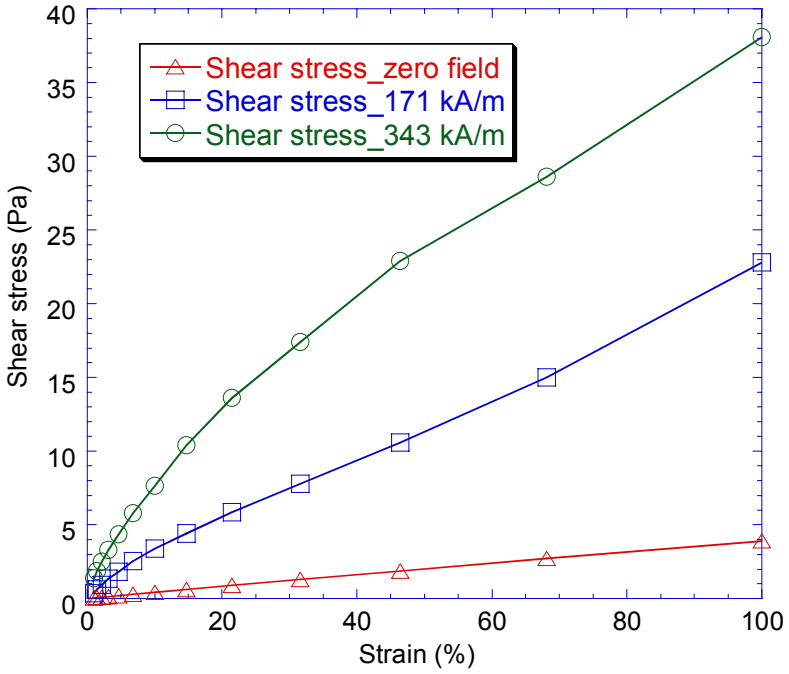

(b)

Fig. 3.2 Strain sweeps for 2.5vol% SWCNT/mo dispersions showing (a) increase in G' and G", and (b) increase in τ with increasing magnetic field.

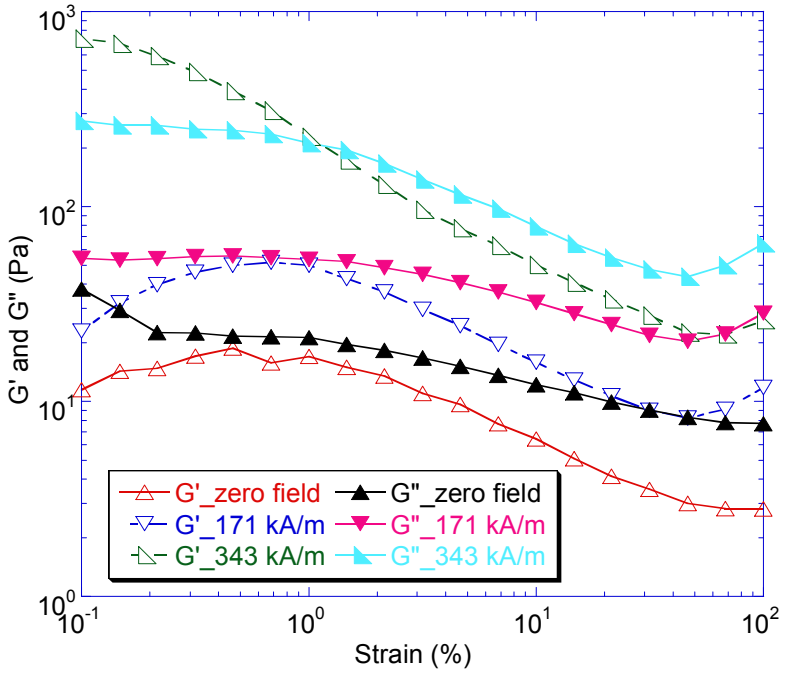

(a)

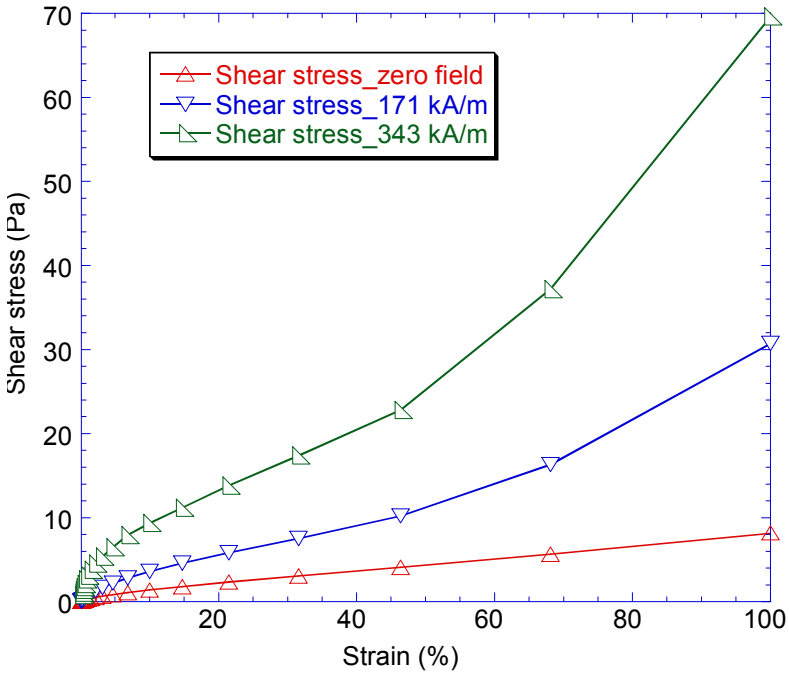

(b)

Fig. 3.3 Strain sweeps for 6.41vol%SWCNT/mo dispersions showing (a) increase in G' and G" with increasing field and one G'-G" crossover, and (b) increase in τ with increasing magnetic field.

Table 3.1 G' at the strain of1% from strain sweeps for SWCNT/mo dispersions.

Magnetic field strength (kA/m)	0	171	343
Magnetic flux density (Tesla)	0	0.215	0.431
G' (1.24vol%SWCNT/mo) (Pa)	1.05	13.7	23.3
G' (2.5vol%SWCNT/mo) (Pa)	1.74	17.1	63.2
G' (6.41vol%SWCNT/mo) (Pa)	17	50	228

Fig.3.4 shows the variation of the γ_c with $H\omega^{-1/2}$ on a log-log scale. The slope of the plot is 0.73, which is slightly smaller than the reported slope of 1 for MR fluids of carbony iron particle/silicon oil investigated by Claracq [38]. In their case, a large volume fraction (up to 30%) of carbonyl iron particles was dispersed in silicone oil while our nanotube concentration is negligibly low. This explains the different slopes observed. Claracq [38] reported that the critical strain could be related to the non dimensional Mason number (Mn) defined as the ratio between hydrodynamic and magnetic stresses. As the field strength increases, the solid-liquid transition occurs at higher strains. The solid-liquid transition is reflective of the presence of a flocculated network.

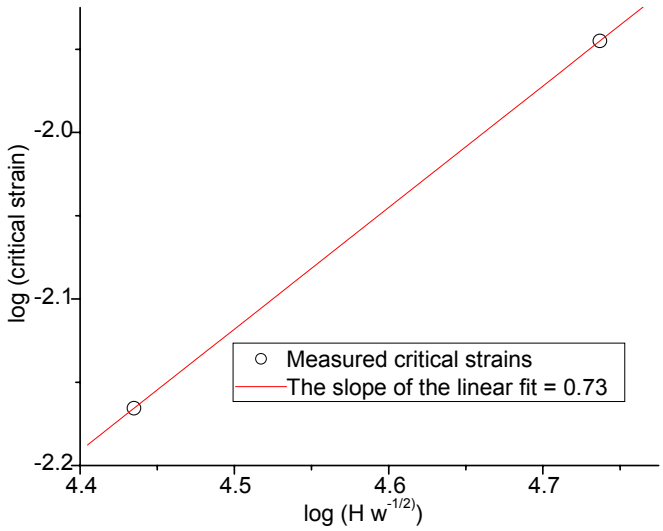

Fig. 3.4 Variation of γ_c versus H and ω from the strain sweeps for 6.41vol%SWCNT/mo.

3.1.2 Frequency Sweeps of SWCNT/mo Dispersions

The results of dynamic frequency sweeps for 1.24vol%, 2.5vol% and 6.41vol% are shown in Fig. 3.5-3.7, respectively. Both G' and G" are observed to be frequency and concentration dependent. We first examine the frequency dependence. For entangled polymer solutions and melts, G' is proportional to ω^2 and G" is proportional to ω. The slopes of log G' vs. logω and log G" vs. logω are tabulated in Table 3.2 from the data of frequency sweeps. For the compositions of 1.24vol% and 2.5vol%, the values mimic that of an entangled polymer solution, and G' increases substantially with increasing frequency. Increasing field strength results in a weaker frequency dependence of both G' and G". For the 6.41vol% composition, deviation from the proportionality is more evident, and G' is totally independent of ω at low frequencies, while exhibiting a strong

dependence at higher frequencies. The frequencies corresponding to the onset of non-Newtonian behavior in applied field strengths of zero, 171, 257 and 343 (kA/m) are 1, 4.64, 10 and 20.1 (rad/s) respectively (Fig. 3.7a). So increasing the magnetic field enhances the elastic response and delays the non-Newtonian behavior. For compositions of 1.24vol% and 2.5vol%, the damping factor, tan δ, decreases with increasing frequency in the absence of an applied field and a peak tan δ is observed under a magnetic field. For the 6.41vol% composition (Fig. 3.7b), a peak tan δ occurs whether or not an external field is applied. The frequencies corresponding to the peak tan δ for SWCNT/mo dispersions are listed in Table 3.3 and they increase with increasing field strength. The relaxation time is inversely proportional to ω and decreases with increasing magnetic field and therefore the dispersion exhibits a more elastic response. There is therefore evidence that the 6.41vol% SWCNT/mo dispersion behaves like a gel. This phenomenon has been observed in concentrated aqueous nanotube dispersions above 0.5vol% studied by Kinloch et al. [29]. Under the application of a magnetic field, the ω^2 dependence dropped closer to one. We surmise that the effect of increasing the field strength leads to the entrapment of the mineral oil between the aligned nanotubes and the increase in elastic properties of the dispersion. We also note that a solid-liquid transition is again evident by examining the crossover of G' and G" as a function of frequency (Table 3.4). In the absence of a field, the crossover frequency increases with increasing SWCNT concentration. In addition, in the presence of an applied field, the crossover frequency increases

with increasing field strength for the same composition. Only one crossover is observed at low nanotube concentrations such as 1.24vol%. At higher concentrations such as 2.5vol%, however, two crossovers are observed for a magnetic field strength of 257 kA/m of larger. At even higher concentrations, two crossovers are evident for 6.41vol%, whether or not an external magnetic field is applied. Both crossover frequencies shift upwards as the field strength is increased. These results indicate that in the absence of a field, the transition to flow behavior occurs due to disentanglement. When a sufficient concentration of nanotubes is present and the nanotubes are aligned perpendicular to the direction of the force, however, there is a two-stage response to the applied force. In the first stage, energy is again consumed in the disentanglement. However the disentangled network then has a secondary region. This may be a region between the nanotubes aligned and nanotubes still bundled in ropes.

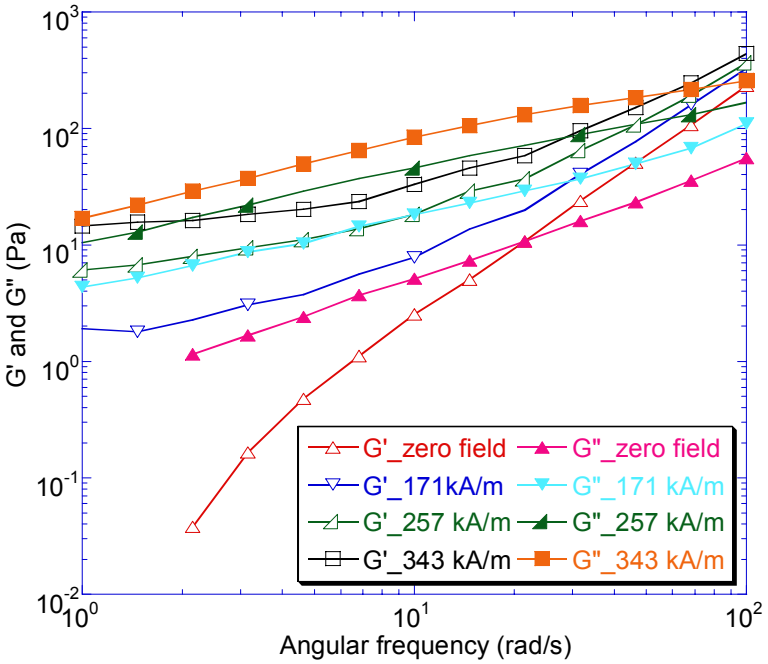

(a)

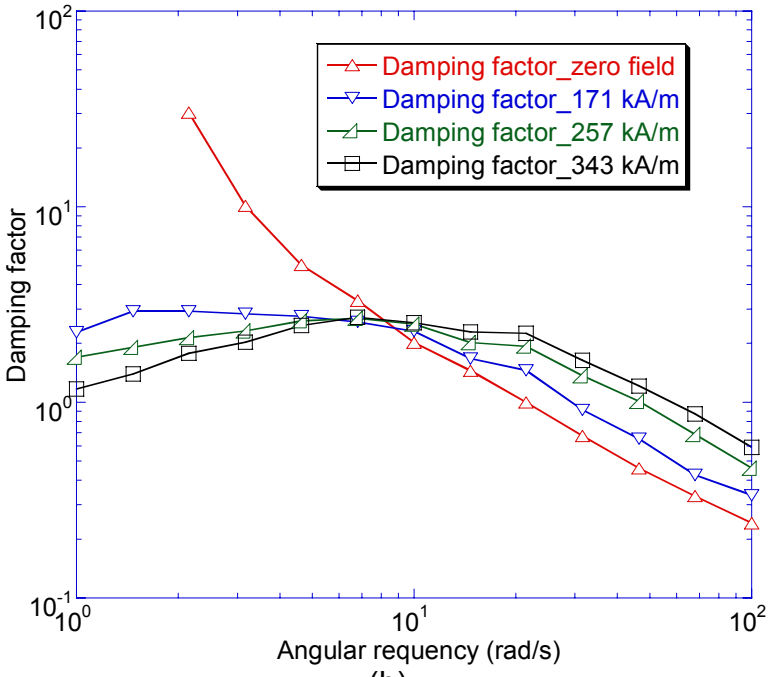

(b)

Fig. 3.5 (a) Frequency sweeps for 1.24vol% SWCNT/mineral oil showing one G'-G" crossover, and (b) The damping factor decreases with increasing magnetic field in low frequency regime.

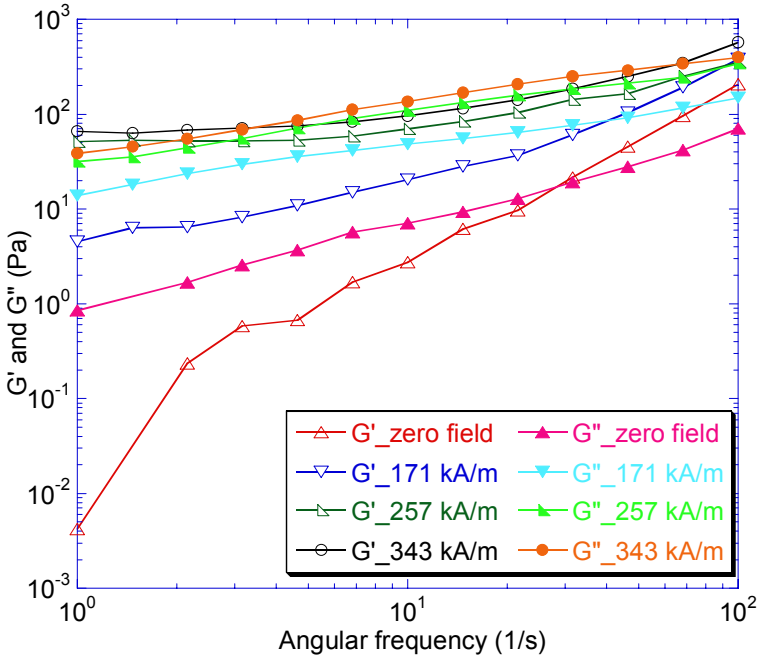

(a)

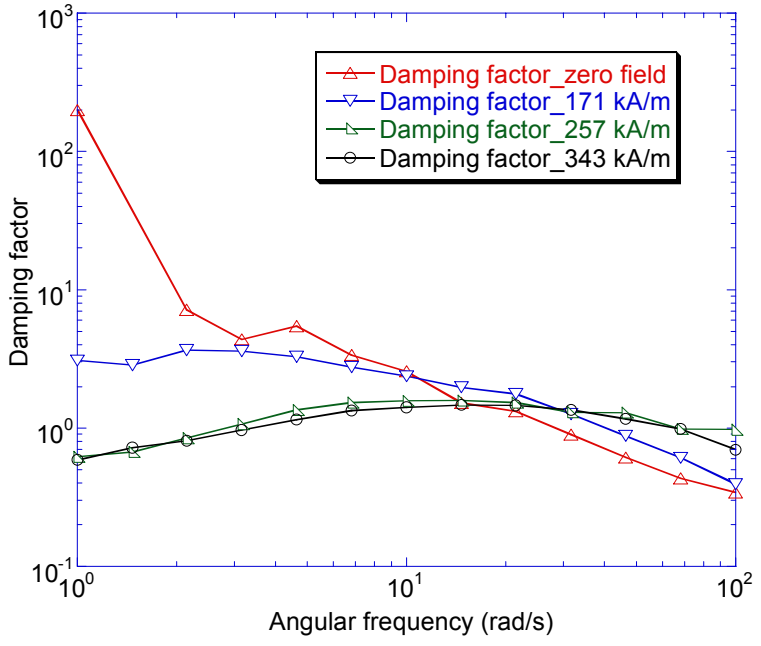

(b)

Fig. 3.6 (a) Frequency sweeps for 2.5vol% SWCNT/mineral oil showing both one and two G'-G" crossovers. The frequency at G'-G" crossover increases with increasing magnetic field, and (b)The damping factor decreases with increasing magnetic field in low frequency regime.

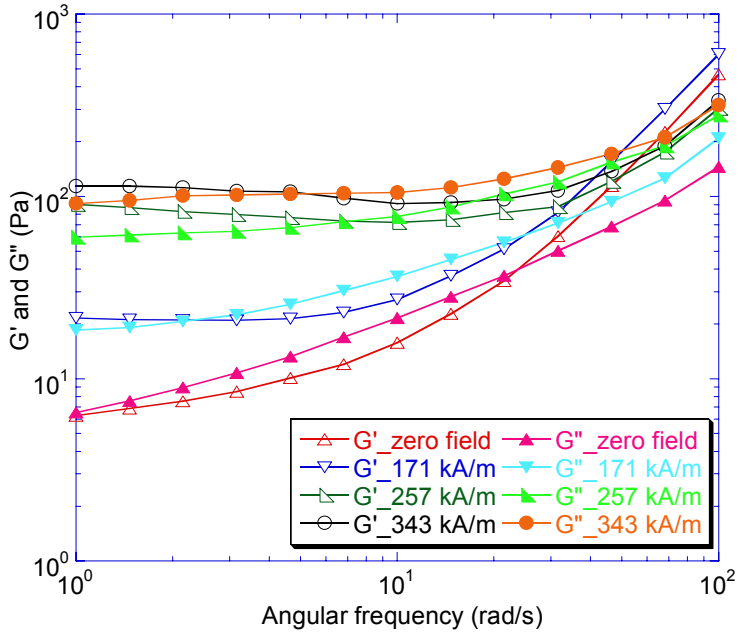

(a)

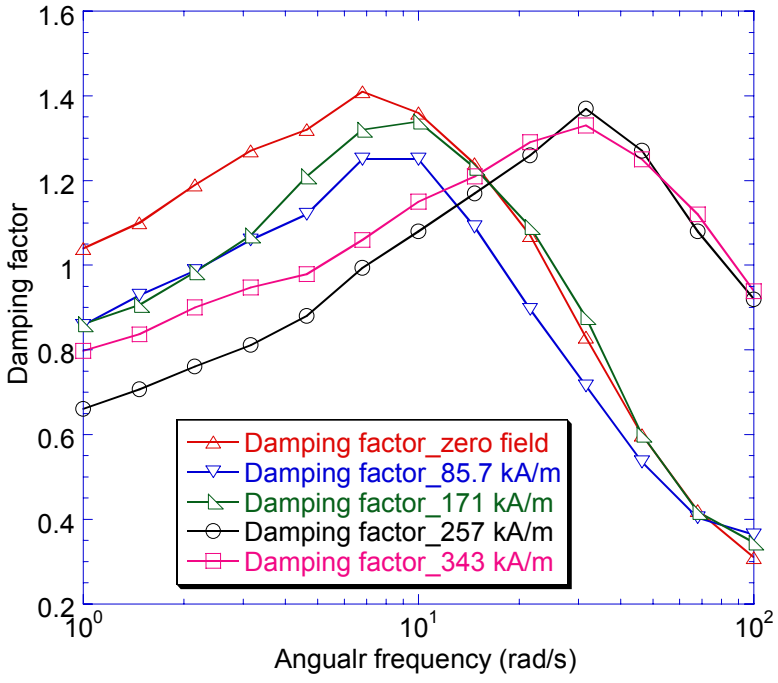

(b)

Fig. 3.7(a) Frequency sweeps for 6.41vol% SWCNT/mo showing two G'-G" crossovers. The frequencies at G'-G" crossovers increase with increasing magnetic field, and (b) The frequency at peak tan δ increases with increasing field.

The slopes of log G' vs. log ω and log G" vs. log ω are tabulated in Table 3.2 from the data of frequency sweeps.

Table 3.2 Slopes of log G' vs. log ω and log G" vs. log ω from the frequency sweeps of SWCNT/mo dispersions

vol% SWCNT/mo	Magnetic field strength (kA/m)	log G' vs. log ω	log G" vs. log ω
1.24	0	2.16	1
1.24	171	1.14	0.68
1.24	257	0.87	0.61
1.24	343	0.73	0.6
2.4	0	2.02	0.92
2.4	171	0.91	0.48
2.4	343	0.45	0.53
6.41	0	0.9	0.67
6.41	171	0.68	0.51
6.41	257	0.18	0.31
6.41	343	0.14	0.22

Table 3.3 Frequencies (rad/s) corresponding to peak tan δ for SWCNT/mo dispersions under different magnetic fields. N/A means no peak tan δ

Magnetic field strength (kA/m)	0	85.7	171	257	343
Magnetic flux density (Tesla)	0	0.108	0.215	0.323	0.431
1.24vol%SWCNT/mo	N/A	N/A	1.47	6.81	6.81
2.5vol%SWCNT/mo	N/A	1.47	2.15	14.7	14.7
6.41vol%SWCNT/mo	6.81	6.81	10	31.6	31.6

Table 3.4 Frequencies (rad/s) corresponding to the G'-G" crossovers for mineral oil and SWCNT/mo dispersions under different magnetic fields.

Magnetic field strength (kA/m)	0	85.7	171	257	343
Magnetic flux density (Tesla)	0	0.108	0.215	0.323	0.431
Mineral oil	14.9		22.8	19.6	
1.24vol%SWCNT/mo	21.8	23.87	30.1	47.8	58.2
2.5vol%SWCNT/mo	28.43	27.2	40.28	2.82, 64.19	3.48, 67.26
6.41vol%SWCNT/mo	1,23.3	2.28,17.87	2.47, 25.72	6.95, 82.14	5.22, 88

In the absence of a field, the crossover frequency increases with increasing SWCNT concentration. As the field strength increases, the crossover frequency increases with increasing field strength for the same composition. Only one crossover is observed at low nanotube concentrations such as 1.24vol%. At higher concentrations such as 2.5vol%, however, two crossovers are observed for a magnetic field strength of 257 kA/m of larger. At even higher concentrations, two crossovers are evident for 6.41vol% whether or not an external magnetic field is applied to the dispersion. Both frequencies at G'-G" crossovers shift to higher frequencies as the field strength is increased. The results indicate that in the absence of a field, the transition to flow behavior occurs due to disentanglement. When a sufficient concentration of nanotubes is present and the tubes are aligned perpendicular to the direction of the force, however, there is a two-stage response to the applied force. First, energy is consumed in the disentanglement. However the disentangled network then has a secondary region. This may be a region between the nanotubes aligned and nanotubes still bundled in ropes.

The frequency sweeps show that both G' and G" increase with increasing magnetic field for all concentrations, especially in the low frequency region. At low concentrations (1.24vol% and 2.5vol%) there is no evident plateau region in the dependence of G' or G" on the frequency. At 6.41vol% however, a plateau region is evident and becomes more pronounced with increasing field strength.

Also, as the applied field strength increases, deviation from Newtonian behavior is delayed to higher frequencies.

Klingenberg [40] and McLeish [39] modeled electrorheological (ER) fluids. If one changes E to H and ε to μ, MR fluids can be modeled in a similar fashion. McLeish et al. [39] distinguished two kinds of chain formation under magnetic field application: chains connected to both electrodes and “free” string chains attached to at most one electrode, with the other end free. Under small amplitude oscillatory shear, the attached chains deform affinely at all oscillation frequencies, producing no relaxation. The storage modulus scales with field strength but is independent of oscillation frequency. The loss modulus arises from free chains and may deform non-affinely depending on the frequency. In another study, Klingenberg (1992) [40] examined structure formation by computational means. The authors found that at moderate to large particle concentration, particle clusters form as opposed to single particle chains. The relaxation process is associated with a frequency dependent dynamic structure within the cluster. The G' scales with the squared field intensity. A transition between the frequency responses is characterized by a characteristic time similar to time-temperature superposition, termed time-field strength contribution. It can be seen that entangled particulate clusters affect the frequency response differently. First, we consider the field intensity scaling. Claracq et al [38] proposed a scaling law to examine the relation between G' and G", the applied field strength, and concentration given by $G \sim (H\varphi)^{1.65}$. At the frequency of 2.15

(rad/s) from the frequency sweep data for 1.24vol%SWCNT/mo, the plot of log G' and log G" vs. log (Hφ), the product of magnetic field strength, H, and volume fraction of SWCNT, φ, is shown in Fig. 3.8.

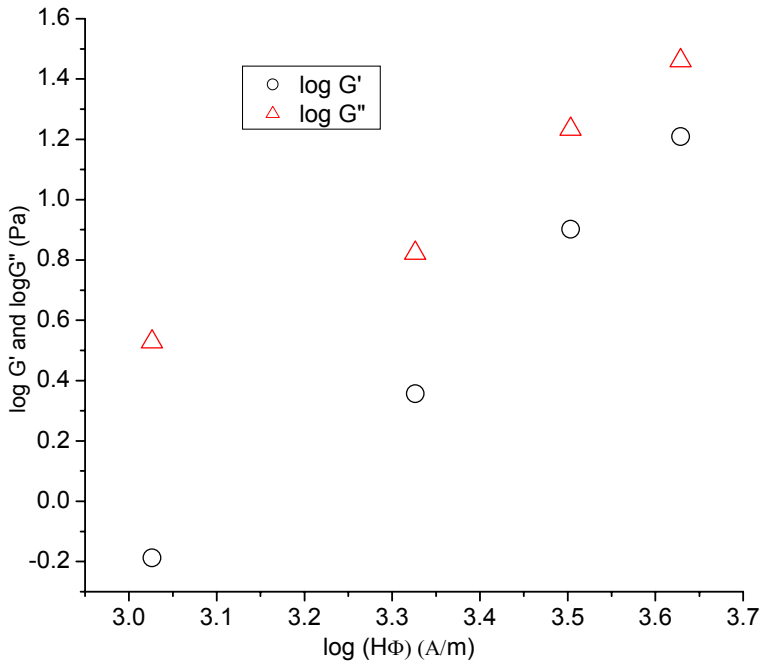

Fig. 3.8 log G' vs. log (Hφ) and log G" vs. log (Hφ) for 1.24vol%SWCNT/mo, indicating a power law relationship between G', G" and Hφ at the frequency of 2.15 (rad/s) from the frequency sweep data. The open circles and triangles represent the measured values.

The slopes for the linear fit for log G' vs. log (Hφ) and log G" vs. log (Hφ) are 2.34 and 1.56 respectively. This shows that G' and G" scale with (Hφ) by a power law: Similarly, the G' and G" are obtained from the frequency sweep data for 2.5vol% and 6.41vol%SWCNT/mo and the results are shown in Fig. 3.9 and Fig. 3.10, respectively. Fig. 3.9 shows log G' vs. log (Hφ) and log G" vs. log (Hφ) for 2.5vol%SWCNT/mo, indicating a power law relationship between G', G" and

(Hφ) at the frequency of 2.15 (rad/s) from the frequency sweep data. The open squares and triangles represent the measured values.

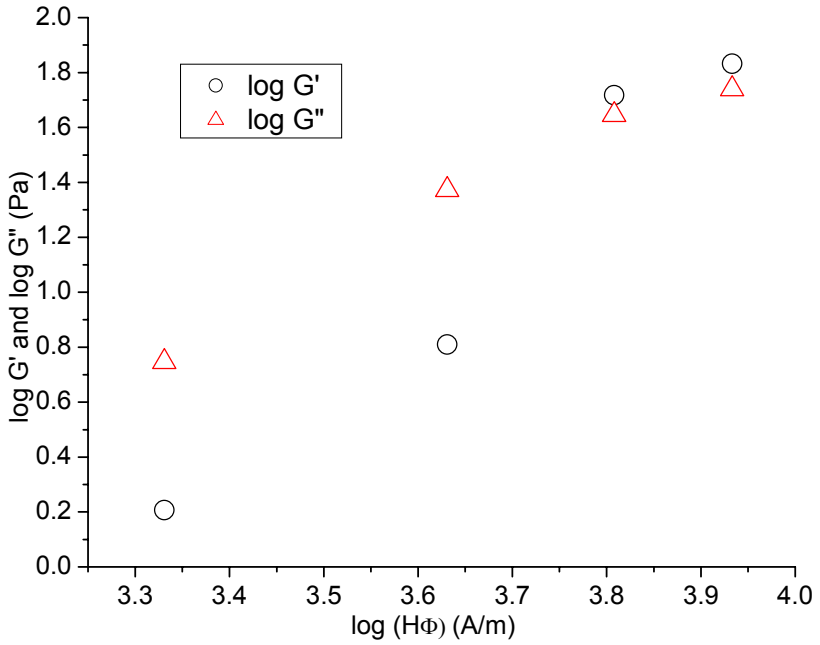

Fig. 3.9 log G' vs. log (Hφ) and log G" vs. log (Hφ) for 2.5vol%SWCNT/mo, indicating a power law relationship between G', G" and (Hφ) at the frequency of 2.15 (rad/s) from the frequency sweep data. The open circles and triangles represent the measured values.

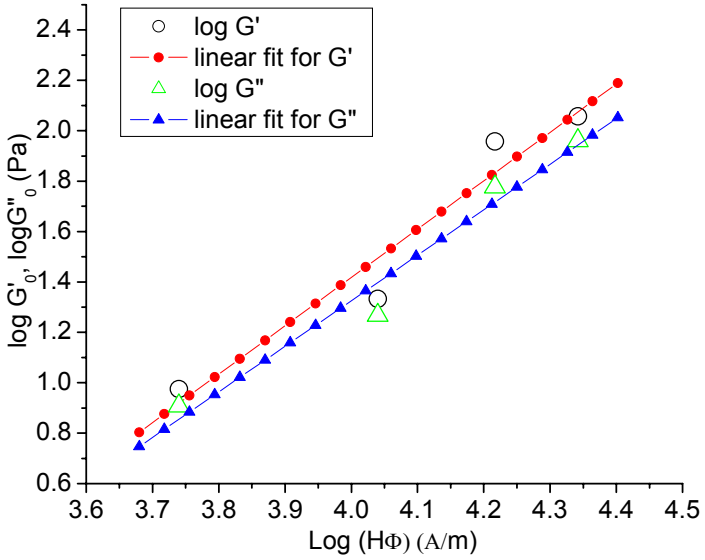

Fig. 3.10 log G' vs. log (Hφ) and log G" vs. log (Hφ) for 6.41vol%SWCNT/mo, indicating a power law relationship between G', G" and Hφ at the frequency of 1 (rad/s) from the frequency sweep data. The open circles and triangles represent the measured values.

The scaling factors obtained in the present investigations are shown below:

$G' \sim (H\varphi)^{2.34}$ for 1.24vol%SWCNT/mo with fit quality R=0.99

$G'' \sim (H\varphi)^{1.56}$ for 1.24vol%SWCNT/mo with fit quality R=0.98

$G' \sim (H\varphi)^{2.89}$ for 2.5vol%SWCNT/mo with fit quality R=0.98

$G'' \sim (H\varphi)^{1.69}$ for 2.5vol%SWCNT/mo with fit quality R=0.99

$G' \sim (H\varphi)^{1.92}$ for 6.41vol%SWCNT/mo with fit quality R=0.98

$G'' \sim (H\varphi)^{1.81}$ for 6.41vol%SWCNT/mo with fit quality R=0.99 (3.1)

From the above indices, we can see that the index of (Hφ) for G' increases with concentration up to 2.5vol% decreases at the concentration of 6.41vol%. In other words, the G' of 2.5vol%SWCNT/mo increases most rapidly

with magnetic field strength, which agrees with the strain sweep results that that composition displays the largest relative increase in G'.

The concentration effect is also separately examined in the absence of a field. The G' and G" increase greatly with increasing nanotube volume fraction, φ. The G' and G" measured at the frequency of 1.59 (rad/s) extracted from the frequency sweep data for 6.41vol% SWCNT/mo are fitted to a power law as shown in Fig. 3.11.

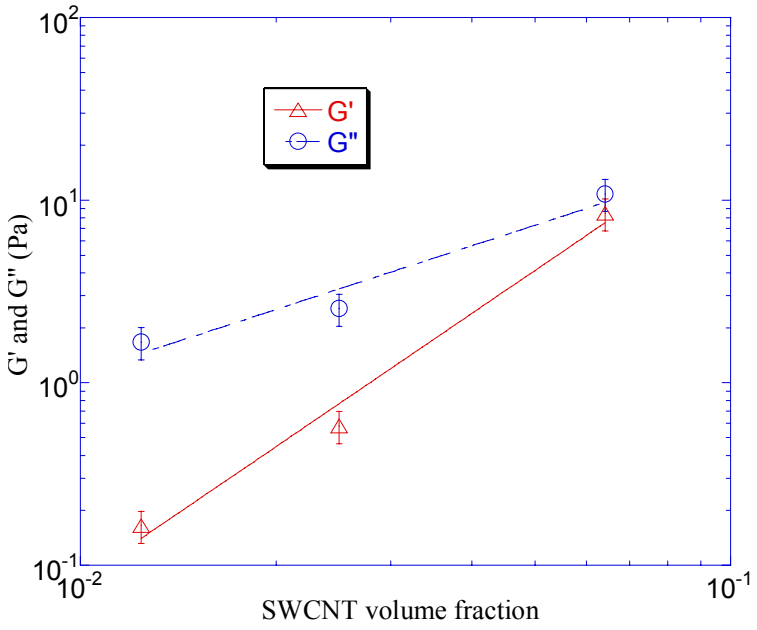

Fig. 3.11 G' and G" vs. φ for 6.41vol% SWCNT/mo from the frequency of 1.59 (rad/s) without a magnetic field. The G' and G" scale with concentration by a power law relationship. The open circles and triangles are measured data, which are fitted to a power law.

The relationships for the data are given by:

$G' = 5854\ \varphi^{2.42}$ with fit quality R=0.999

$G'' = 234\ \varphi^{1.16}$ with fit quality R=0.99 (3.2)

Power law relationship between G and φ has been found theoretically and experimentally for flocculated systems. For the power law index, the experimental values between 2.4 and 4.4 have been reported [37].

3.1.3 Steady Shear Tests of SWCNT/mo dispersions

Steady shear properties are analyzed from the flow curves of the dispersions. Fig. 3.12 shows representative flow curves for the 1.24vol%SWCNT/mo dispersions. The shear stress increases with increasing shear rate and also increases with increasing magnetic field strength at same shear rate, in particular, at low shear rate region.

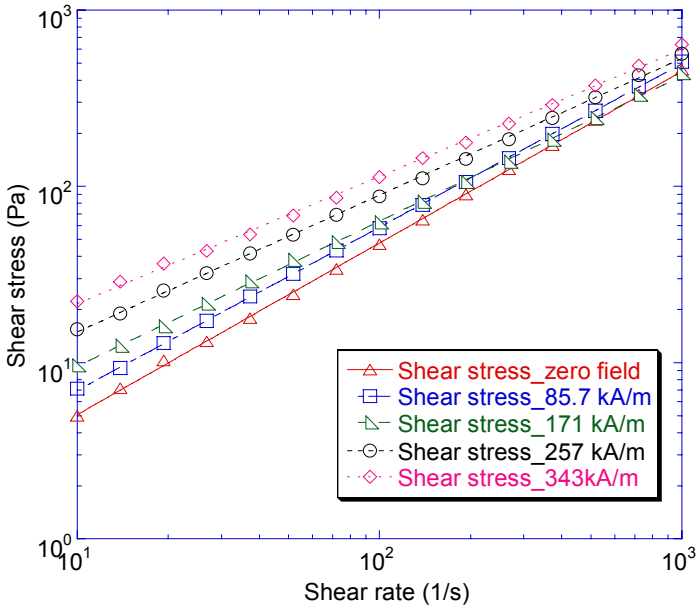

Fig. 3.12 Flow curves for 1.24vol%SWCNT/mo under various magnetic field strength. The measured data are fitted to the power law designated by the lines.

Non-Newtonian flows are often described by the Ostwald-de Waele or so-called power law model:

$$\tau = k\dot{\gamma}^{n}$$

$$\eta = k\dot{\gamma}^{(n-1)} \quad (3.3)$$

Where the constant, k, is the consistency index and represents the viscosity for a Newtonian fluid. The constant, n, is the flow index, which indicates the degree of deviation from Newtonian behavior (n=1). The consistency and flow indices for SWCNT/mo dispersions under various magnetic fields are presented in Table 3.5.

Table 3.5 Consistency (k) and flow (n) index for mineral oil and SWCNT/mo dispersions under different magnetic fields.

Magnetic field strength (kA/m)	0	85.7	171	257	343
Magnetic flux density (Tesla)	0	0.108	0.215	0.323	0.431
k (mineral oil)	0.42		0.4		0.48
n (mineral oil)	0.988		1		0.965
k (1.24vol%SWCNT/mo)	0.54	0.82	1.44	2.5	4.11
n (1.24vol%SWCNT/mo)	0.97	0.93	0.82	0.78	0.72
k (2.5vol%SWCNT/mo)	0.78	0.98	2.6	4.52	10.71
n (2.5vol%SWCNT/mo)	0.92	0.88	0.78	0.69	0.62
k (6.41vol%SWCNT/mo)	4.2	6.81	6.63		9.03
n (6.41vol%SWCNT/mo)	0.85	0.83	0.82		0.76

All power law indices in various magnetic field strengths are less than 1 therefore all systems are pseudoplastics displaying shear thinning. Furthermore increasing the magnetic field increases the k values and decreases the n values for each composition. For instance, n decreases from 0.97 to 0.72 and k

increases from 0.54 to 4.11 when the applied magnetic field strength increases from 0 to 343 kA/m for 1.24vol%SWCNT/mo dispersions.

Following the Bingham model, the yield stress was found for each flow curve by extrapolating the flow curve to zero-shear rate and finding the intersection with the vertical axis and the results are presented in Table 3.6.

Table 3.6 Yield stresses for mineral oil and SWCNT/mo dispersions under various magnetic fields following the Bingham model.

Composition	Magnetic field strength (kA/m)	Magnetic flux density (Tesla)	Yield stress (Pa)
Mineral oil	0	0	0.22
Mineral oil	171	0.215	0.08
Mineral oil	343	0.431	0.55
1.24vol%SWCNT/mo	0	0	1
1.24vol%SWCNT/mo	85.7	0.108	5.5
1.24vol%SWCNT/mo	171	0.215	14.6
1.24vol%SWCNT/mo	257	0.323	24.4
1.24vol%SWCNT/mo	343	0.431	38.5
2.5vol%SWCNT/mo	0	0	2.69
2.5vol%SWCNT/mo	85.7	0.108	3.56
2.5vol%SWCNT/mo	171	0.215	10.85
2.5vol%SWCNT/mo	257	0.323	18.24
2.5vol%SWCNT/mo	343	0.431	43.76
6.41vol%SWCNT/mo	0	0	2.08
6.41vol%SWCNT/mo	85.7	0.108	3.02
6.41vol%SWCNT/mo	171	0.215	2.7
6.41vol%SWCNT/mo	343	0.431	2.8

As seen, the yield stress increases without a field with SWCNT concentration except in the flocculated 6.41vol% dispersion. The field strength dependence on the suspensions indicates difference at lower field strengths but a similar effect at highfield strengths. This is further investigated by a scaling model.

The yield stress measured for a series of applied magnetic flux densities is shown in Fig. 3.13 and fitted to a power-law function of magnetic flux density as follows:

$\tau_y = 121.75\ B^{1.39}$ for 1.24vol%/SWCNT/mo

$\tau_y = 157.52\ B^{1.73}$ for 2.5vol% SWCNT/mo (3.4)

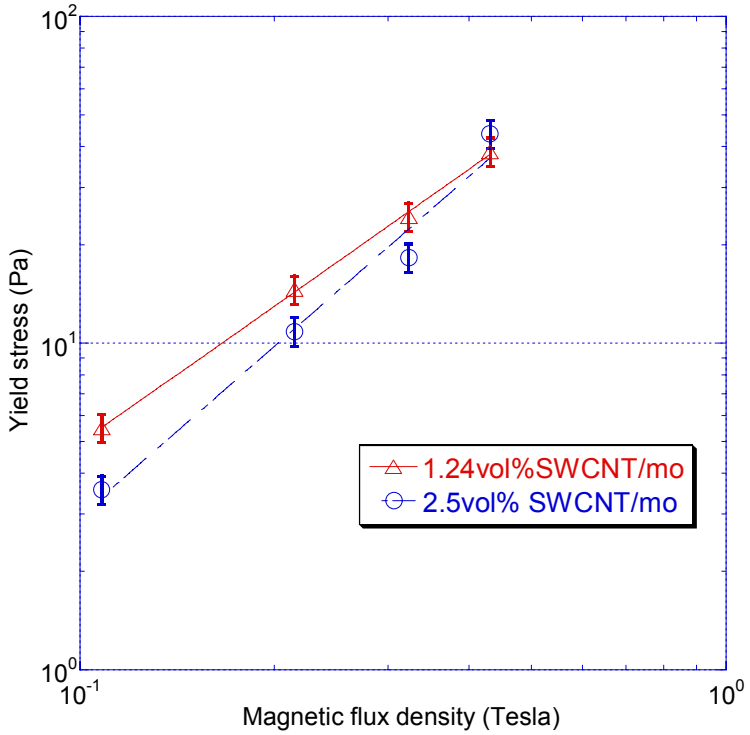

Fig. 3.13 Yield stress vs. magnetic flux density for SWCNT/mo dispersions. Open circles and triangles represent the measured values. The solid line represents the fitted power-law at 25°C. The yield stress increases with flux density roughly as $B^{1.39}$.

2.5vol%SWCNT/mo has a larger index than 1.24vol% SWCNT/mo, indicating that the rate of increase in yield stress increases with concentration of SWCNT in mineral oil up to 2.5vol%. These results are consistent with the strain

sweep results that 2.5vol%SWCNT/mo also shows the largest percent increase in G'. For iron-based magnetorheological (MR) fluids such as an φ=0.4 carbonyl iron particles in poly (dimethyl siloxane) or silicone oil, $\tau_{y\sim} B^{1.5}$ relationship has been observed by Phule and Ginder[31]. They observed a Bingham relationship for both iron-based and ferrite-based MR fluids and found that yield stress increased as $B^{1.5}$ at an applied magnetic flux density below 1 Tesla, which is a consequence of the local saturation of the magnetization in the polar or contact zones of each particles [41].

3.1.4 Magneto Sweeps of SWCNT/mo dispersions

The magneto sweep data for SWCNT/mo dispersions are displayed in Fig. 3.14, 3.15 and 3.16. G', G", η* all increase with linearly increasing magnetic field strength due to the increasing degree of alignment of nanotubes with increasing magnetic field strength.

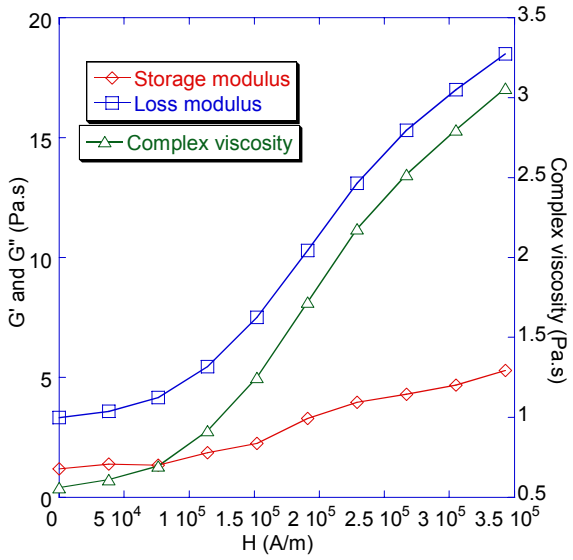

Fig. 3.14 Magneto sweeps for 1.24vol%SWCNT/mo dispersions

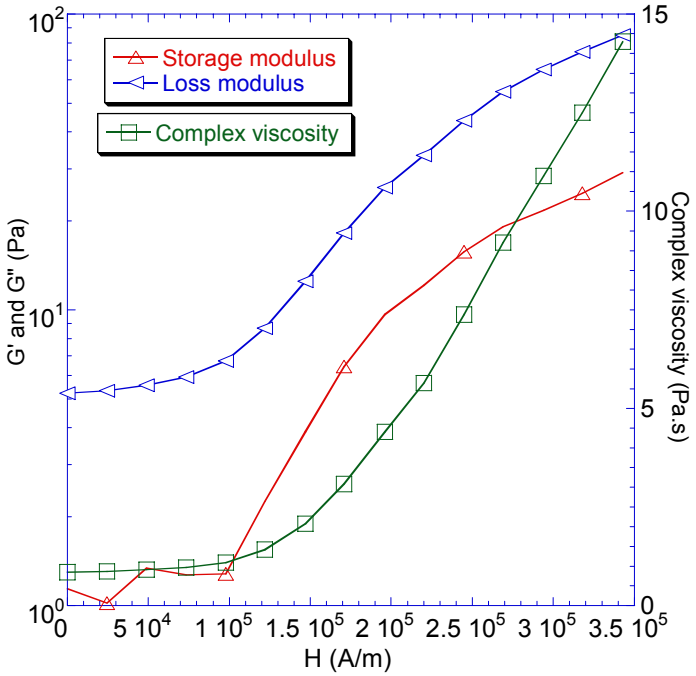

Fig. 3.15 Magneto sweep for 2.5vol%SWCNT/mo dispersions

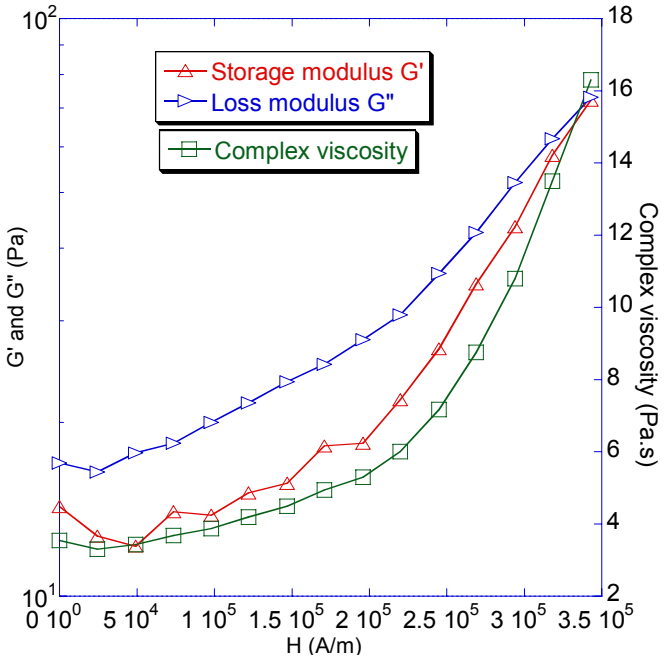

Fig. 3.16 Magneto sweep for 6.41vol%SWCNT/mo dispersions

To have a better view of the effect of the field on the dispersions, values of G', G", η^* obtained during the magneto sweep were normalized by dividing by the corresponding values measured at the beginning of the experiments with zero applied field. The normalized G', G" and η^* are presented in Fig. 3.17. The 2.5vol% composition exhibits the largest relative increase in G', G" and η^* when the magnetic field strength is increased linearly from zero to 343 kA/m. As before (vide supra) the 6.41vol% composition, shows the smallest increase in G', G" and η^*. These results again indicate that residual iron content in the SWCNT is not the main reason for the observed change in properties when the field is applied, are consistent with our observations in the strain sweep experiments. These results indicate rather that a flocculated system is formed at 6.41 vol%, and alignment of the nanotubes is restricted, resulting in gel-like behavior.

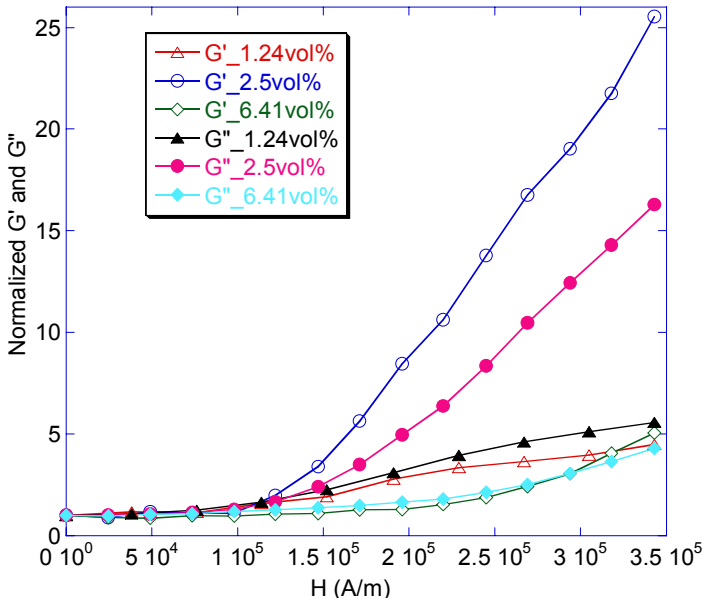

(a)

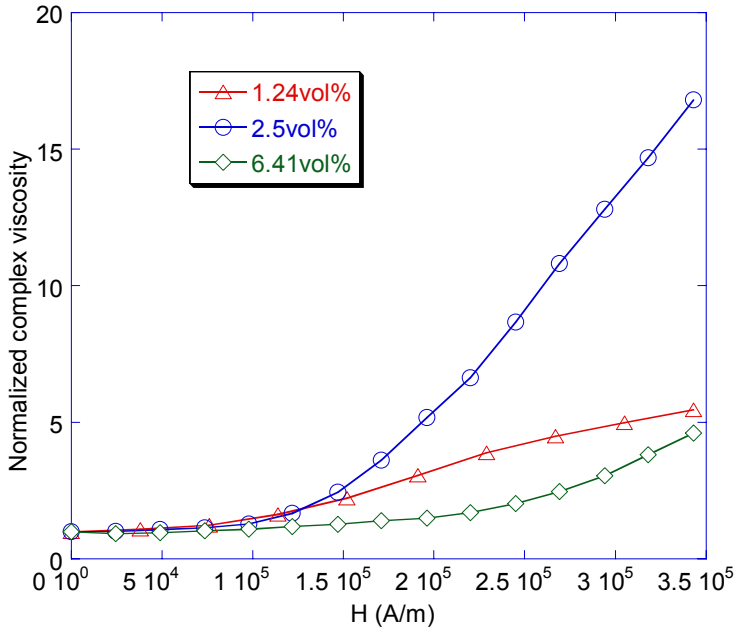

(b)

Fig. 3.17 (a) Normalized G' and G" for SWCNT/mo dispersions (b) Normalized η^* for SWCNT/mo dispersions from the magneto sweep data.

3.1.5 Summary of SWCNT/mo Results

In summary, SWCNTs were aligned by a magnetic field in mineral oil. The extent of alignment increased with increasing magnetic field strength and also increased with nanotube concentration up to 2.5vol% but was the least at the concentration of 6.41vol%. Increasing the magnetic field increased the stiffness of the dispersions. τ_y, G' and G" of SWCNT/mo dispersions increased with increasing magnetic flux density by a power-law relation similar to MR fluids. The shear thinning behavior of SWCNT/mo dispersions followed the power law.

3.2 Single-walled Carbon Nanotube/Epoxy Resin Dispersions

3.2.1 Strain Sweeps of SWCNT/ep dispersions

Fig. 3.18 shows the strain sweep results of 1.68vol%SWCNT/epoxy under different magnetic fields. G' and G" increase slightly with increasing magnetic field.

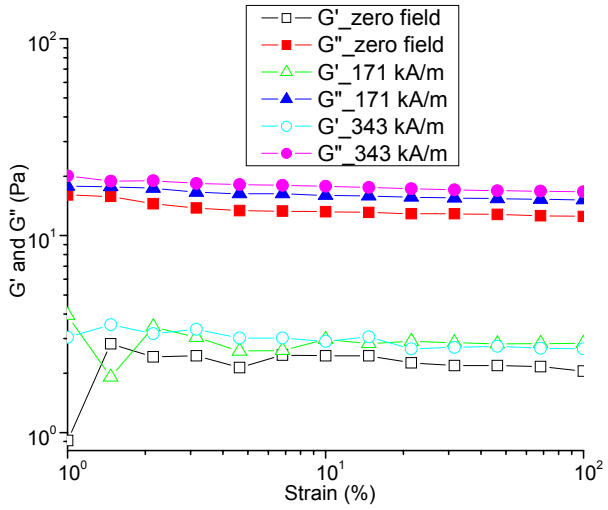

Fig. 3.18 Strain sweeps for 1.68 vol% SWCNT/ep under various magnetic fields.

3.2.2 Frequency Sweeps of SWCNT/ep Dispersions

The frequency sweep curves for neat epoxy resin and 1.68 vol% SWCNT/ep and 3.37 vol.% SWCNT/epoxy are shown in Fig. 3.19. Both G' and G" increase with angular frequency ω. G' and G" of the suspensions are higher than those of neat epoxy and increase with rising SWCNT volume fraction. The slope decreases with increasing SWCNT content indicating rising filler concentration results in less frequency dependence and shear shinning and imparts a largely elastic component to the dispersions.

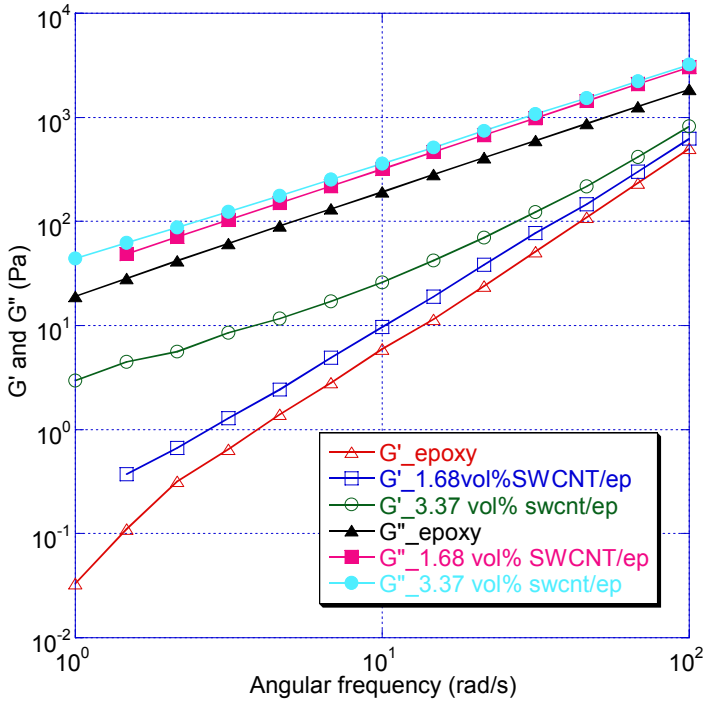

Fig. 3.19 Frequency sweeps for epoxy resin and SWCNT/epoxy dispersions.

η^* of pure epoxy and composites are shown in Fig. 3.20. The complex viscosity increases with nanotube content and the viscosity of 3.37 vol% composition is more than twice as that of pure epoxy. Pure epoxy and 1.68 vol% composions display only weak frequency dependence, showing a Newtonian plateau at low frequencies. At 3.37 vol% SWCNT loading level, a noticeable shear thinning effect is observed. The effect of the nanotubes is more pronounced at low frequencies but the relative effect diminishes with increasing frequency due to shear thinning. This agrees with theoretical expectations and experimental results for fiber-reinforced composites [30], [42].

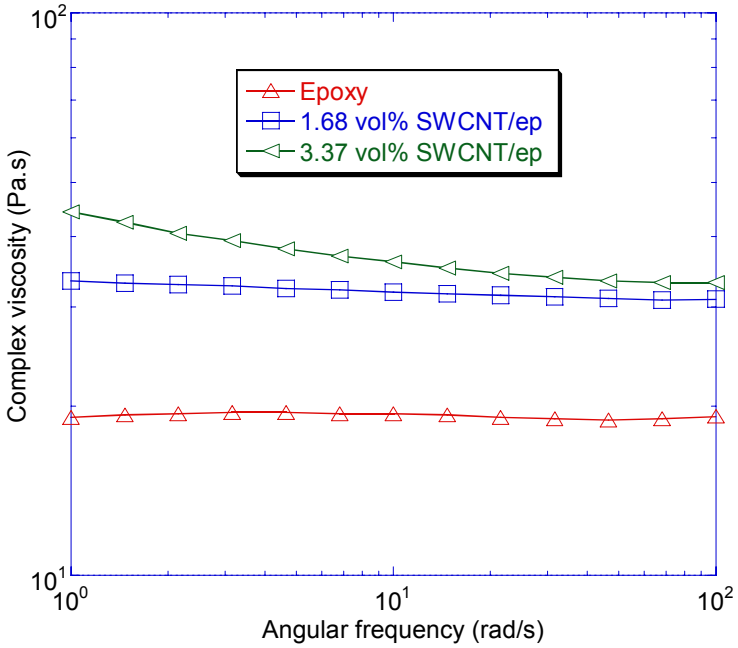

Fig. 3.20 Complex viscosity versus frequency for pure epoxy resin and SWCNT/ep dispersions.

The results for the frequency sweeps for 3.37vol% SWCNT/ep are shown in Fig. 3.21. A very strong shear thinning effect is observed. G' and G" increase slightly with rising magnetic field.

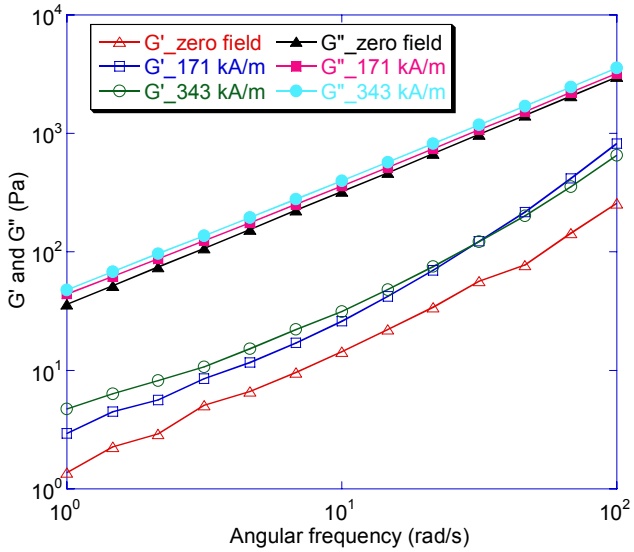

Fig. 3.21 Frequency sweeps for 3.37vol%SWCNT/ep dispersions.

Table 3.7 lists the slope of log G', log G" vs. log ω for epoxy resin and SWCNT/ep dispersions to compare the frequency dependence of the same dispersion under different magnetic fields. Slopes of epoxy resin under various magnetic fields are roughly are the same, indicating the magnetic field has no effect on the epoxy resin, therefore the observed field dependence of SWCNT/ep dispersions results from the response of nanotubes to the magnetic field. Two trends are observed. First, increasing nanotube concentration leads to the decrease in the slope of Log G' vs. log ω in the same field. This implies that the composites become more independent of frequency with increasing nanotube concentration. For instance, 3.37vol% SWCNT/ep is only weakly dependent on the field strength. Indeed nanotubes impart rigidity to the dispersion. Second, the dispersions tend to be less and less dependent on the frequency with increasing magnetic field for the same composition. For example, the slope of log G' vs. log ω decreases from 1.93 to 1.35 when the magnetic field strength increases from zero to 171kA/m for 1.68vol%SWCNT/ep.

Table 3.7 Slopes of log G', log G" vs. log (ω) for SWCNT/ep dispersions from frequency sweeps under various magnetic fields.

Composition	Magnetic field (kA/m)	log G' vs. logω	log G" vs. log ω
Epoxy resin	0	2.05	0.98
Epoxy resin	171	2	1
Epoxy resin	343	2	0.99
1.68vol%SWCNT/ep	0	1.93	0.98
1.68vol%SWCNT/ep	171	1.35	0.97
1.68vol%SWCNT/ep	343	1.4	0.98
3.37vol%SWCNT/ep	0	1.1	0.96
3.37vol%SWCNT/ep	171	1.2	0.93
3.37vol%SWCNT/ep	343	1.06	0.93

3.2.3 Steady Shear Tests of SWCNT/ep Dispersions

Fig. 3.22 shows the flow curves of 1.68vol%SWCNT/epoxy. A small increase in the shear stress with increasing magnetic field strength is observed. Following the Bingham model, the yield stress was found for each flow curve by linearly fitting the low shear rate data and obtaining the linear equation. Table 3.8 lists the yield stress for epoxy resin and SWCNT/ep dispersions under various magnetic fields according to the Bingham model. The yield stress of epoxy resin is only weakly affected by magnetic field stress considering data scattering. Yield stress increases slightly with increasing magnetic field for 1.68vol% and 3.37 vol% SWCNT/ep dispersions.

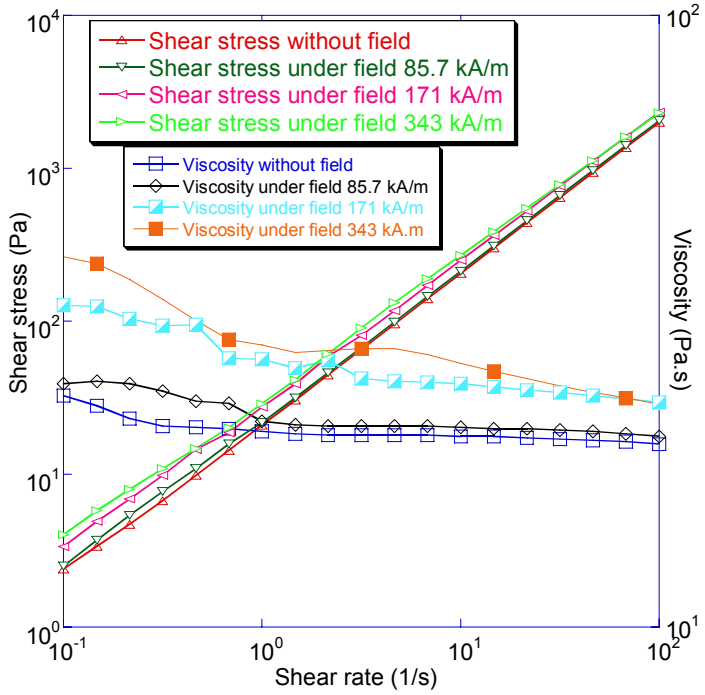

Fig. 3.22 flow curves for 1.68vol%SWCNT/ep dispersions under various magnetic fields.

Table 3.8 Yield stresses for epoxy resin and SWCNT/ep dispersions under various magnetic fields.

Composition	Magnetic field strength (kA/m)	Magnetic flux density (T)	Yield stress (Pa)
Epoxy resin	0	0	0.25
Epoxy resin	85.7	0.108	0.07
Epoxy resin	171	0.215	0.19
Epoxy resin	257	0.323	0.71
Epoxy resin	343	0.431	0.66
1.68vol%SWCNT/ep	0	0	0.35
1.68vol%SWCNT/ep	171	0.215	0.36
1.68vol%SWCNT/ep	343	0.431	1.45
3.37vol%SWCNT/ep	0	0	0.3
3.37vol%SWCNT/ep	171	0.215	0.52
3.37vol%SWCNT/ep	343	0.431	0.86

Fig. 3.23 shows the fit of power law model using flow data with fit quality R larger than 0.99. We can see shear thinning behavior and the flow index n decreases with magnetic field.

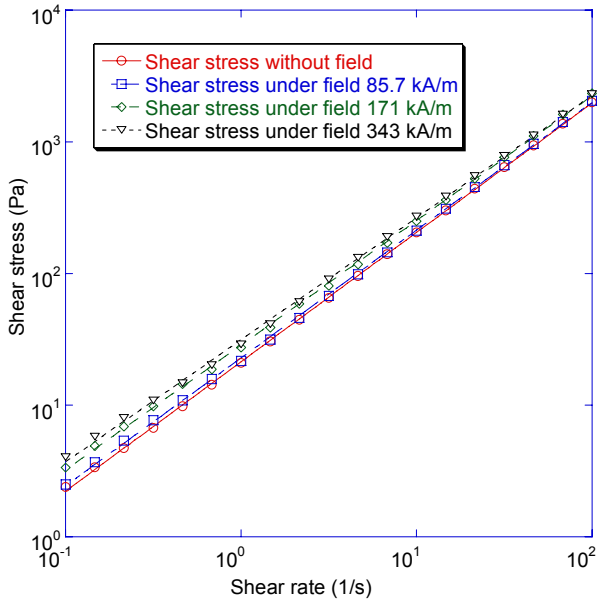

Fig. 3.23 Flow curves for 1.68vol%SWCNT/ep dispersions under various magnetic fields. The open triangles, squares are measured data. The lines show the fit of power law model with fit quality R larger than 0.99.

3.2.4 Magneto Sweeps of SWCNT/ep dispersions

A typical magneto sweep for 3.37vol%SWCNT/ep is shown in Fig. 3.24. G', G" and η^* remain approximately the same below a magnetic field strength of 100000 A/m and then gradually increase with increasing field.

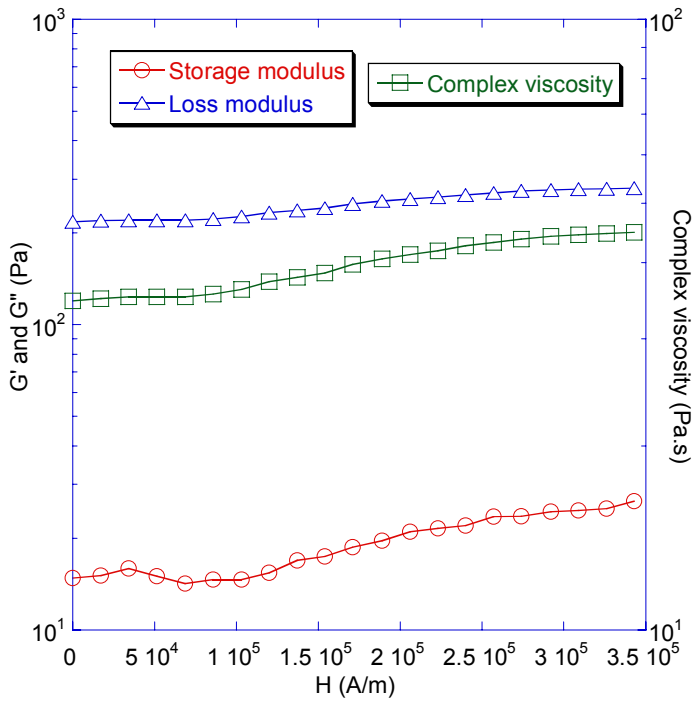

Fig. 3.24 Magneto sweep for a 3.37vol%SWCNT/ep dispersion.

The normalized values, G'/G'_o, G''/G''_o and η^*/η^*_o, for epoxy and SWCNT/epoxy dispersions during magneto sweeps are presented in Fig. 3.25. We note that the effect of magnetic field on the rheological properties SWCNT/epoxy dispersion become noticeable when the magnetic field exceeds around 100kA/m. The rate of increase in G', G" and η^* for 1.68vol% SWCNT/epoxy and 3.37vol% SWCNT/epoxy does not show much difference

except that the latter exhibits higher relative increase in η^* than the former. The increase in G', G",η^* and τ_y of SWCNT/epoxy is partially attributed to increasing alignment of SWCNTs with increasing magnetic field. The magnetic field direction is perpendicular to the two parallel plates and the nanotubes will partially align along the field direction. 3.37 vol% SWCNT concentration is above the reported rheological percolation threshold of 1~2wt%nanotubes [30], at which an interconnected structure of nanotubes begin to form. Therefore the alignment of nanotubes in 3.37 vol% SWCNT/epoxy is restricted.

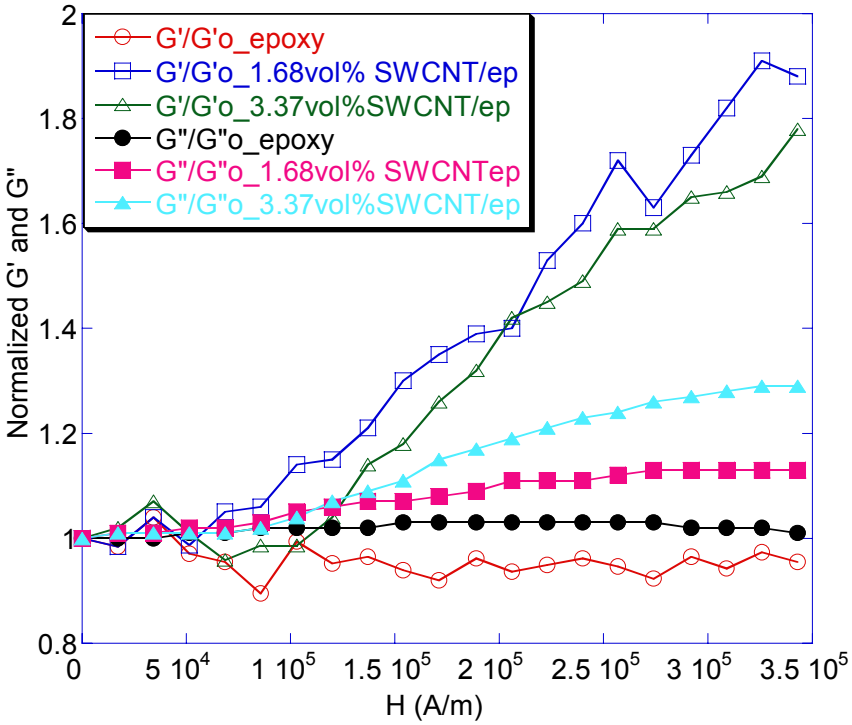

(a)

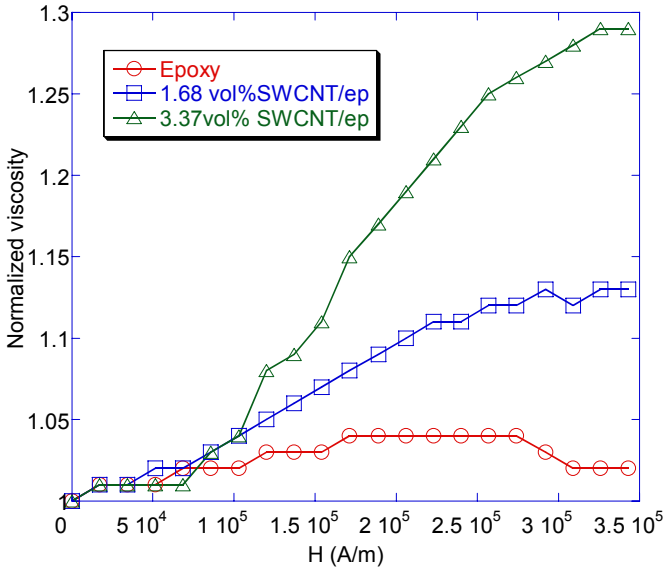

(b)

Fig. 3.25 (a) Normalized G' and G" for epoxy,1.68vol%SWCNT/ep and 3.37vol% SWCNT/ep. (b) Normalized complex viscosity for epoxy, 1.68vol%SWCNT/epoxy and 3.37vol% SWCNT/epoxy using magneto sweep data.

3.2.5 Influence of Dispersion Fluid on MR Response

The viscosity of the supporting liquid for nanotubes also plays an important role in the ease with which the nanotubes can be aligned by the magnetic field in that medium. The shear viscosities of the epoxy resin and mineral oil are 16.7 and 0.42 Pa. s, respectively thus the former is much viscous than the latter. The normalized G', G" and η^* for 1.68vol% SWCNT/ep and 1.24vol%SWCNT/mo from magneto sweeps are shown in Fig. 3.26. We can see 1.24 vol%SWCNT/mo showed a much larger relative increase in G', G" and η^* than 1.68vol% SWCNT/ep. It is more difficult for the nanotubes to be aligned in the epoxy resin than in the mineral oil. On the other hand, nanotubes can rotate more easily in a magnetic field and align along the field direction. Therefore an applied magnetic

field has a larger effect on SWCNT/mo dispersions than SWCNT/ep counterparts.

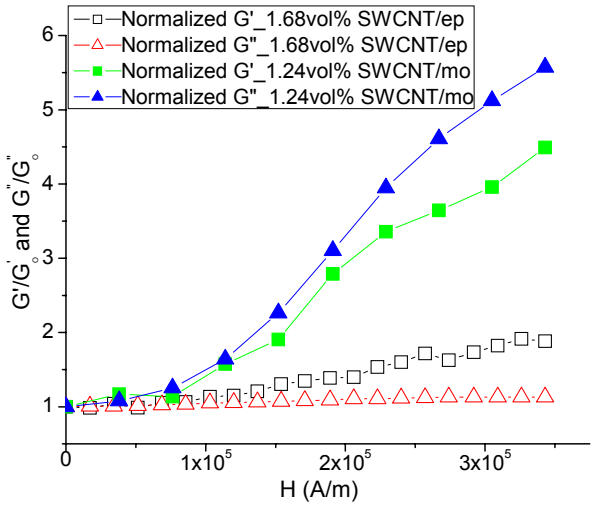

(a)

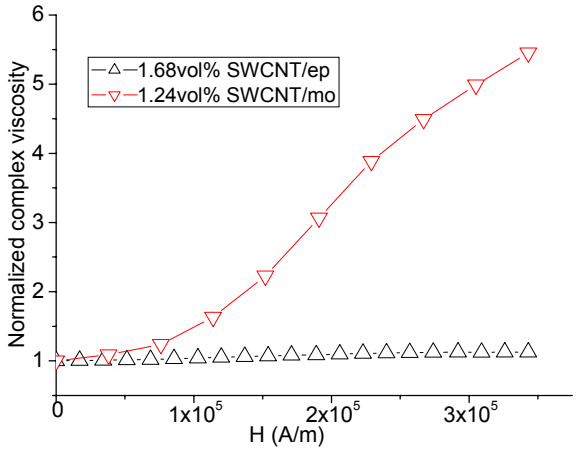

(b)

Fig. 3.26 Normalized G' and G" for 1.68vol% SWCNT/ep and 1.24vol%SWCNT/mo (b) normalized η*for 1.68vol% SWCNT/ep and 1.24vol%SWCNT/mo using magneto sweep data.

3.3 Multi-walled Carbon Nanotube/Mineral Oil Dispersions

3.3.1 Strain Sweeps of MWCNT/mo Dispersions

The strain sweeps for MWCNT/mo dispersions are shown in Fig. 3.27, Fig. 3.28 and Fig. 3.29. The values of G' at the strain of 1% are listed in Table 3.9. For the nanotube concentrations of 0.5 vol%, G" is larger than G' indicating the viscous component of dispersion is dominant. With even higher nanotube concentration such as1.5vol%, G' and G" are comparable and a G'-G" crossover is observed. At low nanotube concentrations, increasing the field strength increases G', G" and τ. The increase is roughly linear. The results indicate that the alignment of the tubes perpendicular to the plates leads to increases in complex shear moduli. At the highest nanotube concentration of 2.53vol%, however, G' first increases and then remains constant with increasing magnetic field. A G'-G" crossover implying a solid-liquid transition is evident in 1.5 and 2.53 vol% dispersions. The strain at the G' -G" crossover is defined as the critical strain, $\gamma_{c.}$ These critical strains are listed in Table 3.10 for all MWCNT/mo dispersions. The tendency is that the critical strain decreases with increasing nanotube concentration in the same magnetic field and also decreases with increasing magnetic field for the same composition and the solid-liquid transition occurs at lower strains. In the case of 2.53 vol% composition, the critical strains under magnetic fields of zero, 171kA/m and 343kA/m are 0.422%, 0.333% and 0.165% respectively. These are in contrast with the strain sweep results of SWCNT/mo dispersions where critical strains of SWCNT/mo dispersions increased with increasing magnetic field for the same composition. We attribute the difference to the higher η^* of MWCNT/mo than SWCNT/mo counterparts.

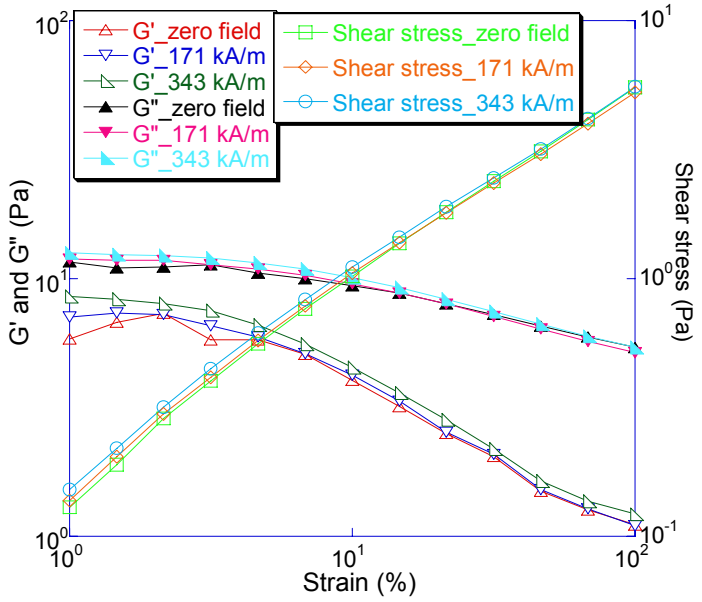

Fig. 3.27 Strain sweeps for 0.5vol% MWCNT/mo under various magnetic fields.

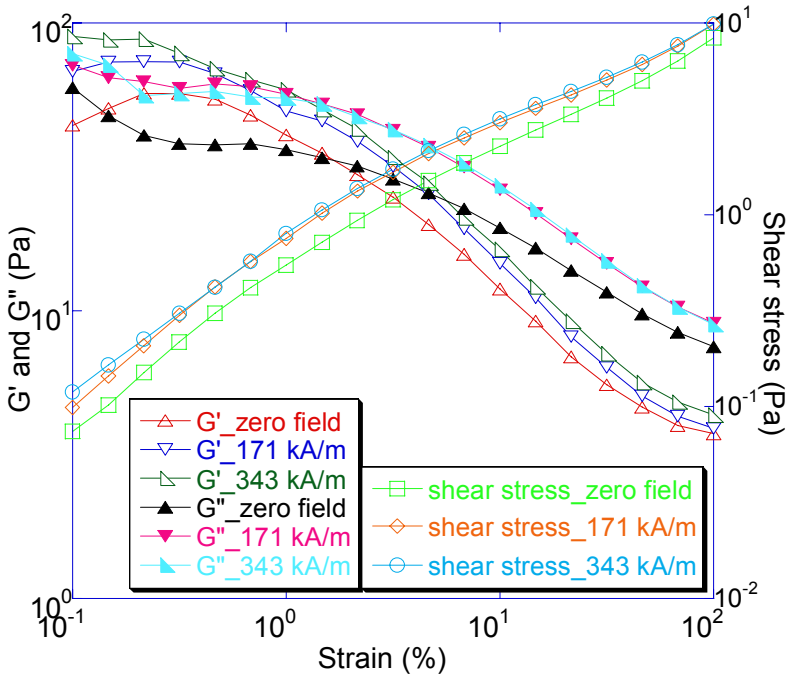

Fig. 3.28 Strain sweeps for 1.5vol%MWCNT/mo showing one G'-G" crossover.

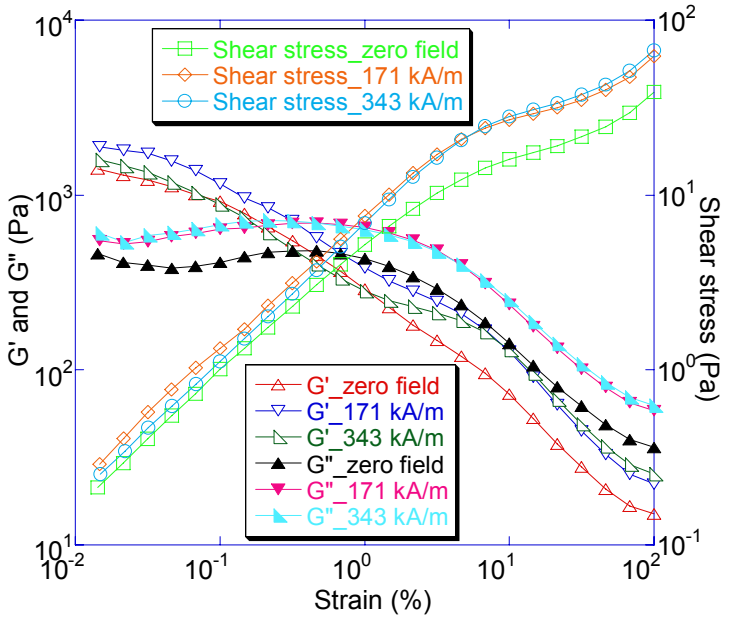

Fig. 3.29 Strain sweeps for 2.53vol%MWCNT/mo dispersions under various magnetic fields showing one G'-G" crossover.

Table 3.9 G' at strain of 1% for strain sweeps of MWCNT/mo dispersions

Magnetic field strength (kA/m)	0	171	343
Magnetic flux density (Tesla)	0	0.215	0.431
G' (0.5vol%MWCNT/mo) (Pa)	5.8	7.1	8.5
G' (1.5vol%MWCNT/mo) (Pa)	40.8	49.5	58.6
G' (2.53vol%MWCNT/mo) (Pa)	290	384	283

Table 3.10 Critical strain γ_c during strain sweeps for MWCNT/mo dispersions under various magnetic fields.

Sample	Magnetic field strength (kA/m)	Magnetic flux density (Tesla)	Critical strain γ_c
1.5vol%MWCNT/mo	0	0	1.64%
1.5vol%MWCNT/mo	171	0.215	0.61%
1.5vol%MWCNT/mo	343	0.431	1.26%
2.53vol%MWCNT/mo	0	0	0.42%
2.53vol%MWCNT/mo	171	0.215	0.33%
2.53vol%MWCNT/mo	343	0.431	0.17%

3.3.2 Frequency Sweeps of MWCNT/mo Dispersions

The frequency sweeps for 0.5, 1.5 and 2.53 vol% MWCNT/mo dispersions

are shown in Fig. 3.30, Fig. 3.31, Fig. 3.32, respectively. At 0.5vol% MWCNT/mo, the magnetic field has very weak effect on G' and G" and the two curves are almost identical. Tan δ also decreases little with increasing magnetic field. At 1.5vol%, both G' and G" increase with magnetic increasing field. At 2.53vol%, G' dominates over G" and tan δ decreases with increasing magnetic field. Increasing the loading of nanotubes and field strength increases the elastic properties. G' and G" are a function of frequency and increases with increasing frequency. The behavior is concentration dependent. At low concentrations of 0.5 and 1.5vol%, the dispersions behave like entangled polymer solutions. However, at a higher concentration such as 2.53vol%, G' and G" have a weak dependence on frequency, especially in the low frequency region.

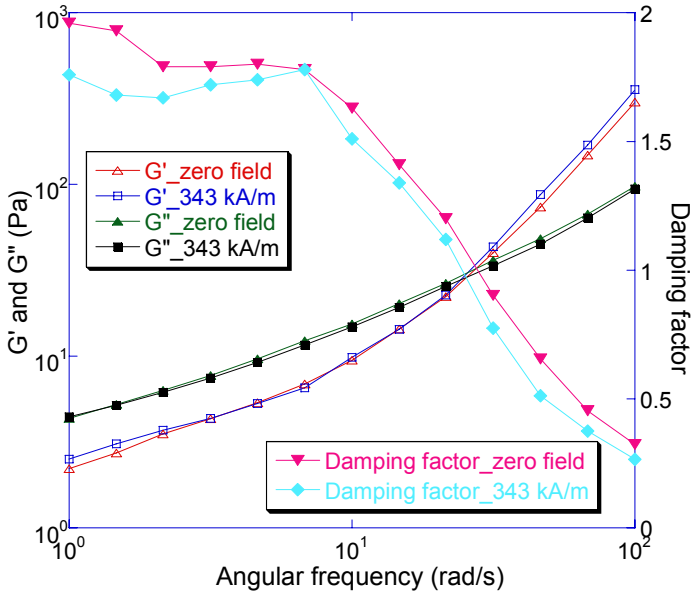

Fig. 3.30 Frequency sweeps for 0.5vol% MWCNT/mo under various magnetic fields.

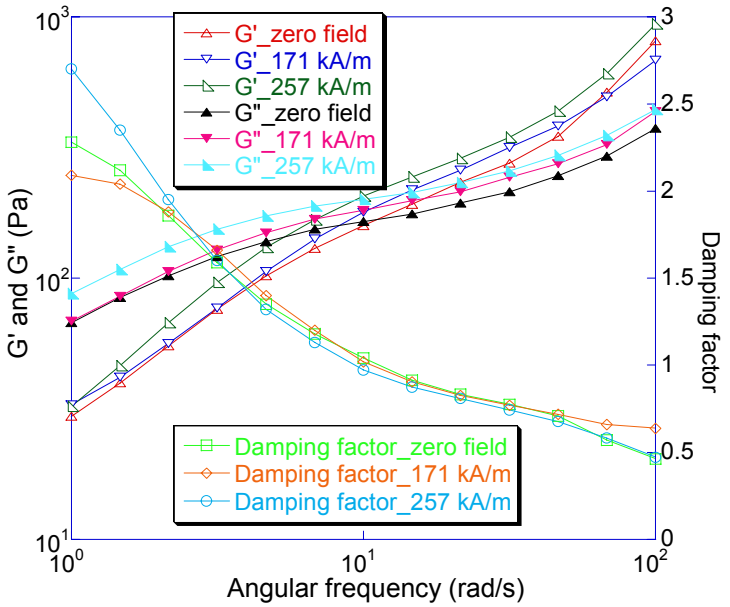

Fig. 3.31 Frequency sweeps for 1.5vol% MWCNT/mo dispersions under various magnetic fields.

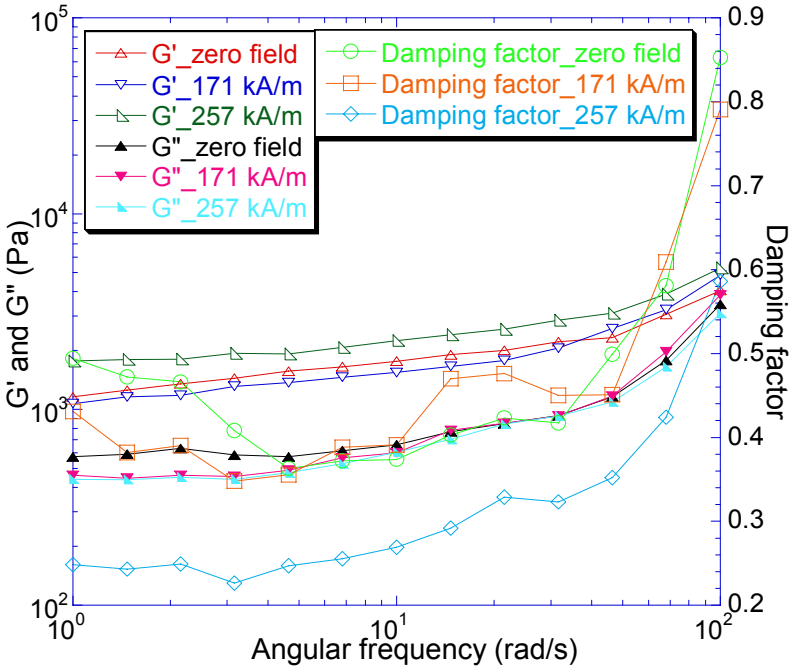

Fig. 3.32 Frequency sweeps for 2.53vol% MWCNT/mo dispersions under various magnetic fields.

A G'-G" crossover is observed for the compositions of 0.5vol% and 1.5vol%. The G'-G" crossover frequencies are listed in Table 3.11. In the absence of a field, the crossover frequency decreases with increasing nanotube concentration. As the field strength increases, the crossover frequency decreases with increasing field strength.

Table 3.11 Angular frequency ω (rad/s) at G'-G" crossover for Mineral oil and MWCNT/mo dispersions under different magnetic fields.

Magnetic field strength (kA/m)	0	171	257	343
Magnetic flux density (Tesla)	0	0.215	0.323	0.431
mineral oil (rad/s)	14.9	22.8	19.6	
0.5vol%MWCNT/mo	28.18			24.48
1.5vol%MWCNT/mo	11.36	10.58	9.38	10

We also note that G' and G" increase dramatically with increasing nanotube volume fraction, φ. The G' and G" measured at the frequency of 1 (rad/s) from frequency sweep data are fitted to a power law as shown in Fig. 3.33. The relationships for the data are given by:

$G' = 3.58e^{8}\varphi^{3.63}$ with fit quality R=0.99

$G'' = 2.15e^{7}\varphi^{2.93}$ with fit quality R=0.99 (3.5)

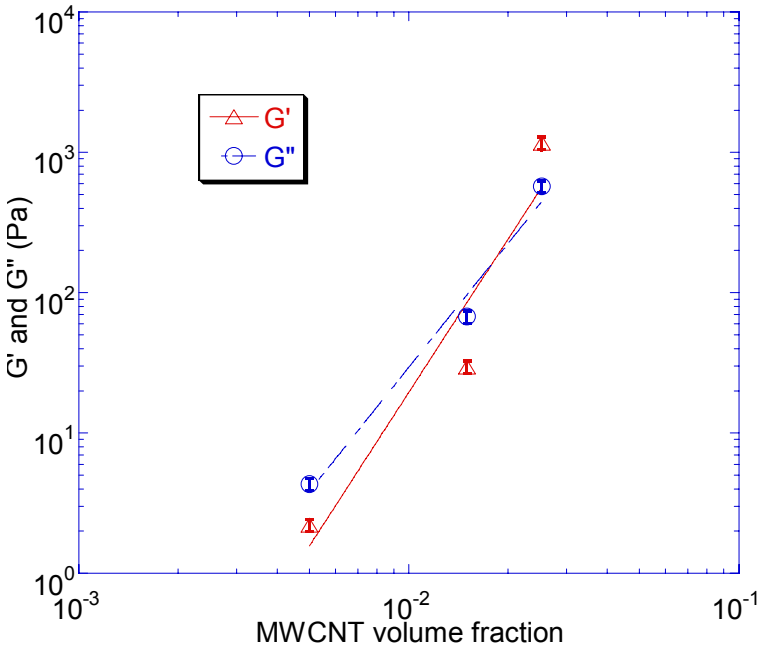

Fig. 3.33 G' and G" as a function of MWCNT concentration in mineral oil. The open triangles and circles are measured values, which are fitted to the power law designated by the lines.

3.3.3 Steady Tests of MWCNT/mo Dispersions

Steady shear properties are analyzed from the flow curves of the dispersions. Fig. 3.34, Fig. 3.35 and Fig. 3.36 show typical flow curves of MWCNT/mo dispersions. The shear stress increases with increasing shear rate and also increases slightly with increasing magnetic field strength at the same shear rate for nanotube concentrations up to 1.5vol%. At a concentration of 2.53vol%, a more pronounced increase in shear stress with increasing magnetic field at the same shear rate is observed.

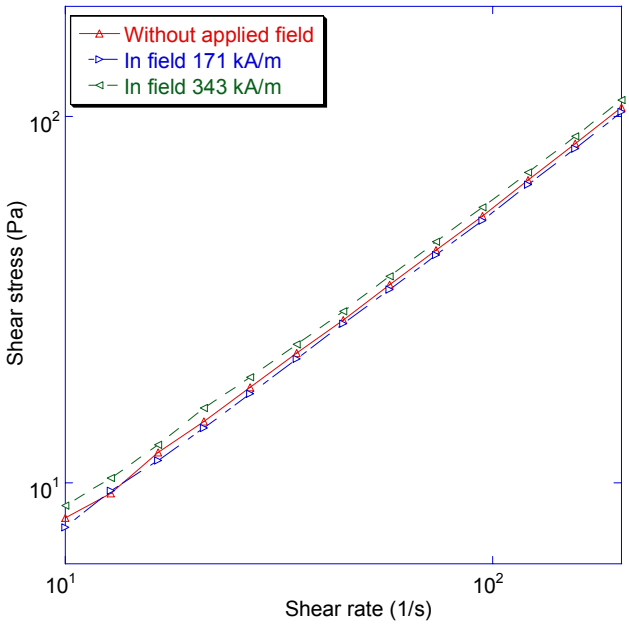

Fig. 3.34 Flow curves of 0.5vol% MWCNT/mo dispersions under various magnetic fields.

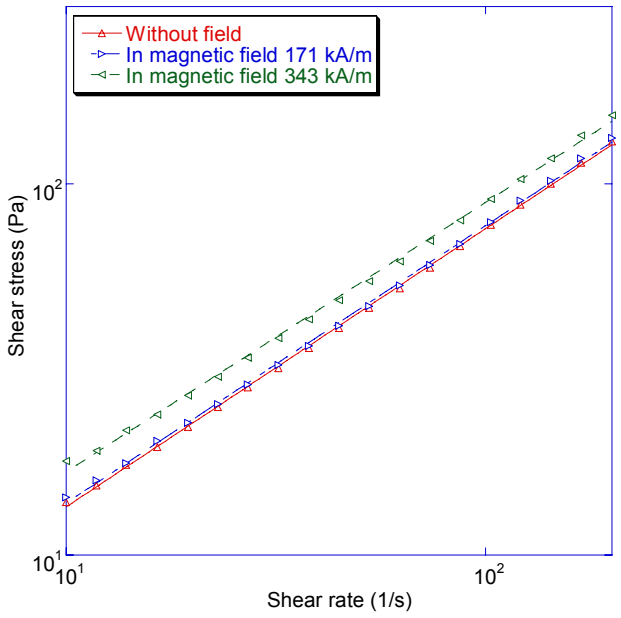

Fig. 3.35 Flow curves for 1.5vol%MWCNT/mo dispersions under various magnetic fields.

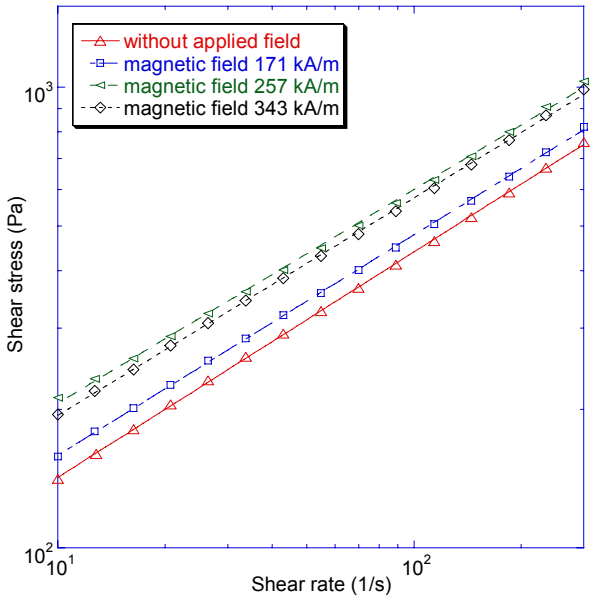

Fig. 3.36 Flow curves of 2.53vol%MWCNT/mo dispersion under various magnetic fields.

Following the Bingham model, the yield stress is obtained by extrapolating the shear stress-shear rate data to zero shear rate and finding the intersection with the vertical axis and the results are presented in Table 3.12.

Table 3.12 Yield stresses for MWCNT/mo dispersions under various magnetic fields.

Sample	Magnetic field strength (kA/m)	Magnetic flux density (Tesla)	Yield stress (Pa)
0.5vol%MWCNT/mo	0	0	1.9
0.5vol%MWCNT/mo	171	0.215	1.982
0.5vol%MWCNT/mo	343	0.431	2.238
1.5vol%MWCNT/mo	0	0	5.58
1.5vol%MWCNT/mo	171	0.215	5.95
1.5vol%MWCNT/mo	343	0.431	8.21
2.53vol%MWCNT/mo	0	0	89.29
2.53vol%MWCNT/mo	171	0.215	103.13
2.53vol%MWCNT/mo	257	0.323	146.55
2.53vol%MWCNT/mo	343	0.431	130.33

The yield stress increases substantially with increasing nanotube concentration and also increases with increasing magnetic field at the same concentration. The obtained yield stresses for different magnetic flux densities are fitted to the power law as shown in Fig. 3.37. The scaling factors are shown below:

$\tau_y \sim 2.59B^{0.17}$ for 0.5vol%MWCNT/mo dispersion

$\tau_y \sim 12.1B^{0.46}$ for 1.5vol%MWCNT/mo dispersion

$\tau_y \sim 388.8B^{0.86}$ for 2.53vol%MWCNT/mo dispersion (3.6)

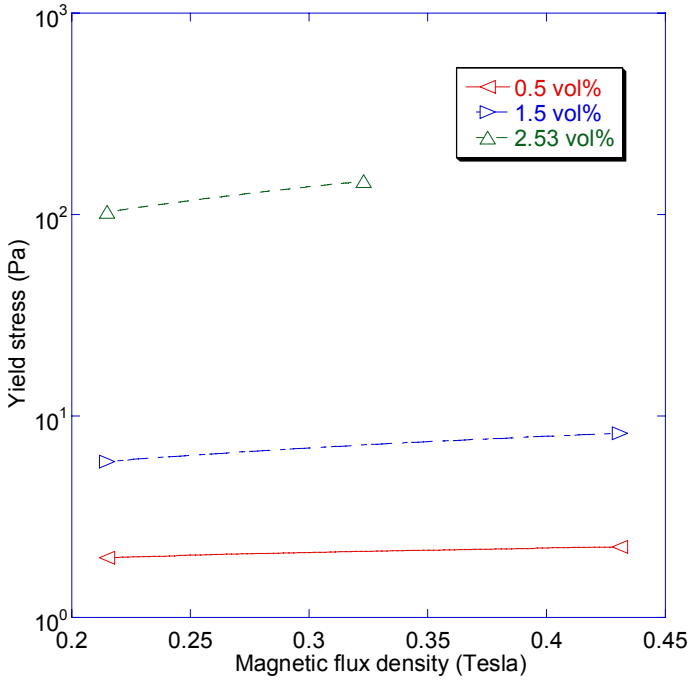

Fig. 3.37 Yield stress versus magnetic flux density for MWCNT/mo dispersions. The open triangles represent measured yield stresses which are fitted to a power law.

Both the coefficients and indices for the yield stress increase with increasing concentration. The obtained data from flow curves are fitted the power

law model. The values of consistency index, k, and flow index, n, for MWCNT/mo dispersions are presented in Table 3.13.

Table 3.13 Consistency indices and flow indices obtained from flow curves for MWCNT/mo dispersions under various magnetic fields.

Magnetic field strength (kA/m)	0	171	343
Magnetic flux density (Tesla)	0	0.215	0.431
k (0.5 vol% MWCNT/mo)	1.052	1.01	1.17
k (1.5 vol% MWCNT/mo)	2.4	2.47	3.15
k (2.53 vol% MWCNT/mo)	46.14	52.81	65.45
n (0.5 vol% MWCNT/mo)	0.866	0.868	0.854
n (1.5 vol% MWCNT/mo)	0.75	0.748	0.726
n (2.53 vol% MWCNT/mo)	0.489	0.479	0.472

We can see all power law indices of MWCNT/mo dispersions under various magnetic fields are less than 1; therefore, all systems are pseudoplastics, which display shear thinning. Furthermore, increasing magnetic field slightly decreases n and increases k. For instance, n decreases from 0.489 to 0.472 and k increases from 46.14 to 65.45 when the applied magnetic field strength increases from 0 to 343 kA/m for 2.53vol%MWCNT/mo dispersions. In the same magnetic field, increasing nanotube concentration increases the k values but decreases the n values.

3.3.4 Magneto Sweeps of MWCNT/mo Dispersions

A magneto sweep for 0.5vol% MWCNT/mo is displayed in Fig.3.38. G', G", and η^* increase weakly with rising magnetic field strength. The normalized G', G" and η^*during magneto sweeps are shown in Fig. 3.39. The lowest nanotube concentration, 0.5vol%, exhibits the largest percent increase in G', G" and η^* while the highest nanotube concentration, 2.53vol%, displays the lowest

relative increase when the magnetic field strength increases linearly from zero to 343 kA/m. This is due to the fact that increasing the nanotube loading in mineral oil results in a dramatic increase in the viscosity of the dispersion and hinders the mobility of MWCNTs. At 2.53 vol%, a flocculated system is formed where nanotubes closely touch each other and rotation of nanotubes along the field direction is seriously restricted. The results agree with the magneto sweep results for SWCNT/mo dispersions. In both case, the highest nanotubes concentrations, namely, 6.41vol%SWCNT/mo and 2.53vol%MWCNT/mo, exhibit the smallest relative increase in G', G" and η^* with increasing magnetic field strength because both viscous dispersions behave like a gel. Both results indicate that it is the alignment of nanotubes by the magnetic field, not the iron content in the naotubes, that is the main reason for the observed increase in G', G" and η^*.

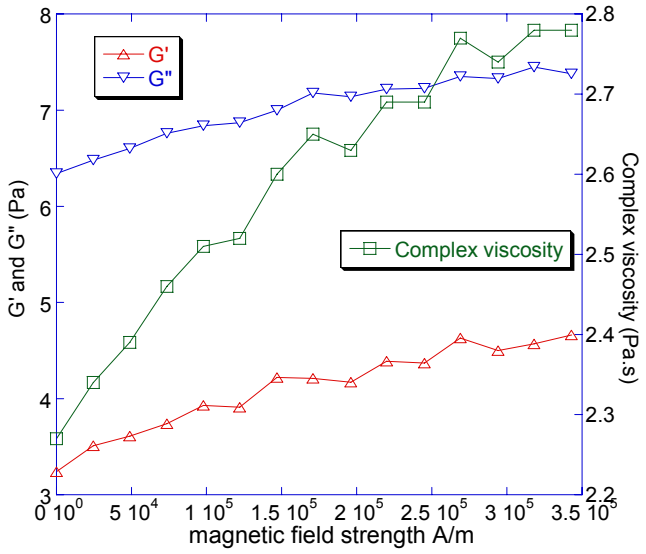

Fig. 3.38 Magneto sweep for a 0.5vol%MWCNT/mo dispersion.

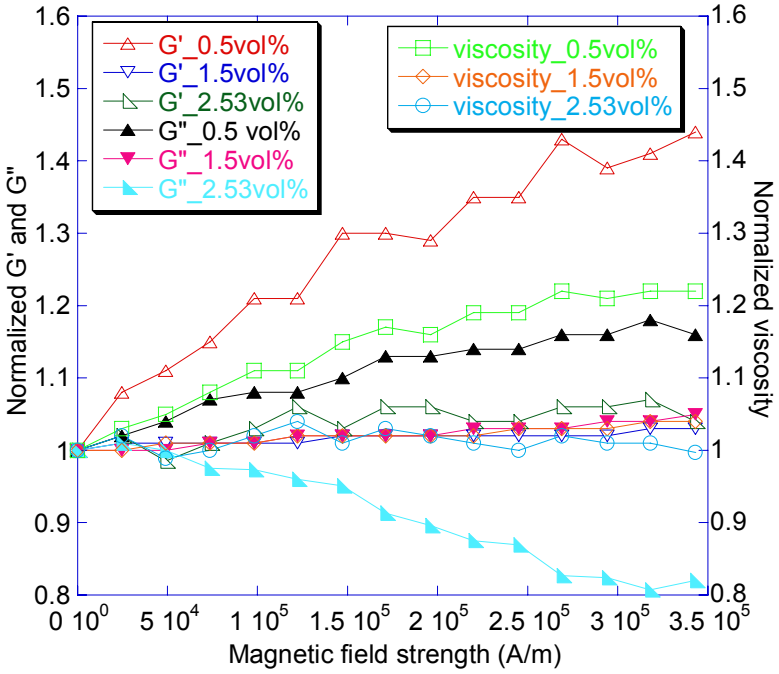

Fig. 3.39 Normalized G', G", η* for MWCNT/mo dispersions from magneto sweeps.

3.3.5 Comparison between MWCNT and SWCNT/mo Dispersions

There are some differences and similarities between the magnetorhelogical behaviors of MWCNT/mo and SWCNT/mo dispersions. First, the strain sweeps show the critical strain increases in a stronger magnetic field for 6.41vol% SWCNT/mo while the opposite trend is observed for 1.5 and 2.53vol%MWCNT/mo dispersions. The G' at a small strain of 1% increase in a stronger field for all SWCNT/mo dispersions while the G' first increases then becomes roughly constant with increasing field for 2.53vol% MWCNT/mo. Second, frequency sweeps show two G'-G" crossovers for 2.5vol% SWCNT/mo under a magnetic field strength of 257 kA/m or higher. For 6.41vol%SWCNT/mo, two G'-G" crossovers are also evident whether or not an external magnetic field

is applied to the dispersions. The frequencies at G'-G" crossovers increase with increasing SWCNT concentration in the same field and also increase with increasing magnetic field strength for the same composition. The two frequencies at the two G'-G" crossovers shift to higher frequencies as the field strength is increased. In contrast, only one G'-G" crossover is observed for 1.5vol% and 2.53vol% MWCNT/mo. The crossover frequency decreases with increasing nanotube concentration in the same field and also decreases with increasing magnetic field strength. The G' and G" of the SWCNT/mo dispersions are more and more independent of the angular frequency, especially in low frequency regime, under increasing magnetic field while MWCNT/mo dispersions display very little similar trend. In other words, the SWCMT/mo dispersions exhibit more pronounced response to an increasing magnetic field than MWCNT/mo counterparts. Third, from flow curves, SWCNT/mo dispersions show much larger extent by which the shear stress increases with increasing magnetic field at the same shear rate for the same composition than MWCNT/mo dispersions. The yield stress of SWCNT/mo dispersions increases more rapidly than MWCNT/mo with increasing magnetic field. The following scaling factors show SWCNT/mo dispersions have larger indices than MWCNT/mo counterparts:

$\tau_y \sim 121.75\ B^{1.39}$ for 1.24vol%/SWCNT/mo

$\tau_y \sim 157.52\ B^{1.73}$ for 2.5vol% SWCNT/mo

$\tau_y \sim 2.59 B^{0.17}$ for 0.5vol%MWCNT/mo

$\tau_y \sim 12.1B^{0.46}$ for 1.5vol%MWCNT/mo

$\tau_y \sim 388.8B^{0.86}$ for 2.53vol%MWCNT/mo (3.6)

Fourth, the SWCNT/mo dispersions display much larger relative increase in G', G" and η^* than MWCNT/mo from the magneto sweeps. Again, we compare the normalized G', G" and η^* for SWCNT/mo and MWCNT/mo dispersions with roughly the same nanotube volume fraction. The relative increase in G', G" and η^* for 1.24vol% SWCNT/mo is around 5 times that for 1.5vol% MWCNT/mo as shown in Fig. 3.40. The relative increase in G', G" and η^* for 2.5vol% SWCNT/mo is around 10-15 times that for 2.53vol% MWCNT/mo as shown in Fig. 3.41.

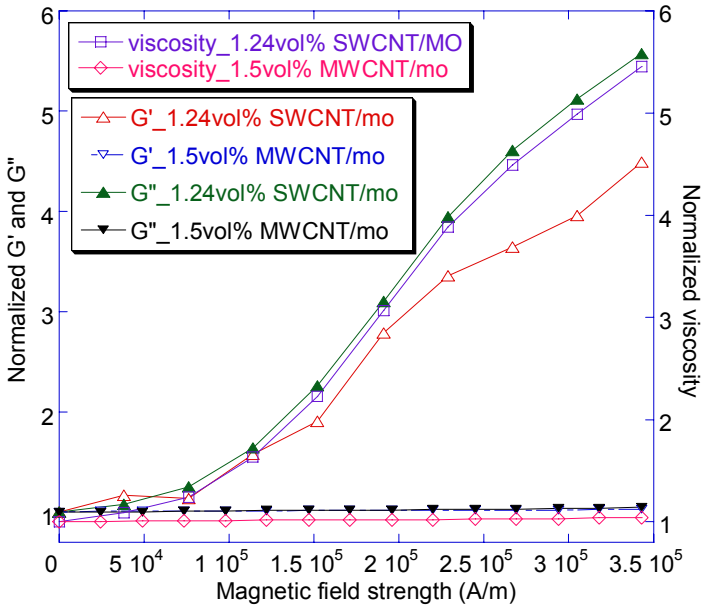

Fig. 3.40 Normalized G', G" and η^* for 1.24vol% SWCNT/mo and 1.5vol% MWCNT/mo during magneto sweeps.

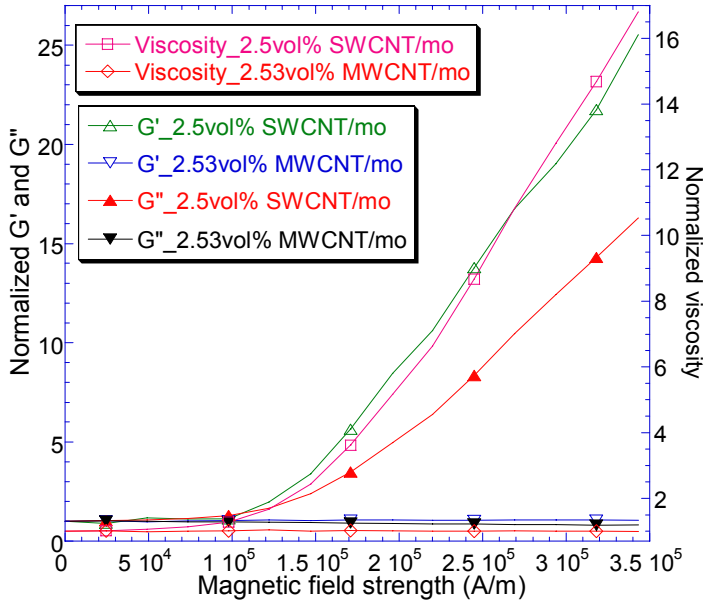

Fig. 3.41 Normalized G', G" and η^* for 2.5vol% SWCNT/mo and 2.53vol% MWCNT/mo during magneto sweeps.

There is a common feature shared by the SWCNT/mo and MWCNT/mo dispersions. The highest nanotubes concentrations, 6.41vol%SWCNT/mo and 2.53vol%MWCNT/mo, exhibit the smallest relative increase in G', G" and η^* during magneto sweeps. Generally, the MWCNT/mo dispersions display much weaker response to an applied magnetic field than SWCNT/mo dispersions mainly because the former has much higher viscosity than the latter at the comparable nanotube concentration. For example, the complex viscosities of 1.24 and 2.5vol% SWCNT/mo dispersion in a zero field are 0.56 and 0.85 Pa. s, respectively while the complex viscosities of 1.5vol% and 2.53vol% MWCNT/mo dispesions are 50.6 and 281 Pa.s, respectively. The viscosity of the medium in which the nanotubes are dispersed plays a vital role in the alignment of nanotubes. The second reason is that SWCNTs used in the experiments

assemble as bundles or ropes and bundles of nanotubes require a less magnetic field than an individual nanotube as suggested by Walters [23].

3.4 Multi-walled Carbon Nanotube/Epoxy Resin Dispersions

3.4.1Strain Sweeps of MWCNT/ep Dispersions

The strain sweeps for 0.67 and 2vol% MWCNT/ep dispersions are shown in Fig. 3.42 and Fig. 3.43 respectively. The numerical values of the G' and G" at the strain of 1% are listed in Table 3.14. The G' and G" increase sharply with increasing nanotube concentration and the modulus for 2vol% are one order of magnitude higher than those for 0.67vol% at low strain region. At the same nanotube concentration, both G' and G" increase with increasing magnetic field. At the nanotube concentration of 0.67vol%, the G' is about one order of magnitude lower than the G", indicating that the viscous component is dominating. Increasing nanotube content enhances the elastic properties and a G'-G" crossover is evident for the 2vol% MWCNT/ep dispersion. The critical strain decreases with increasing magnetic field as shown in Table 3.15, which agrees with the field dependence of critical strains for MWCNT/mo dispersions.

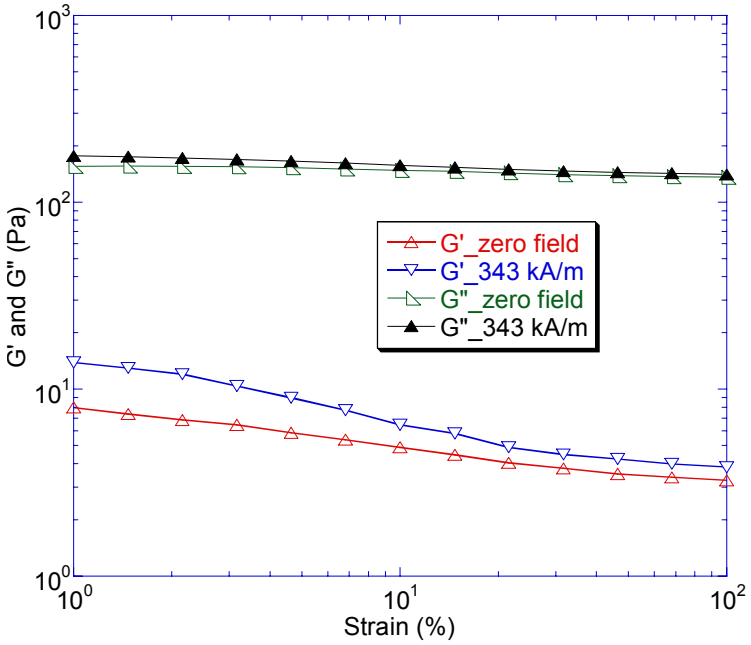

Fig. 3.42 Strain sweeps for 0.67vol% MWCNT/ep dispersions under various magnetic fields.

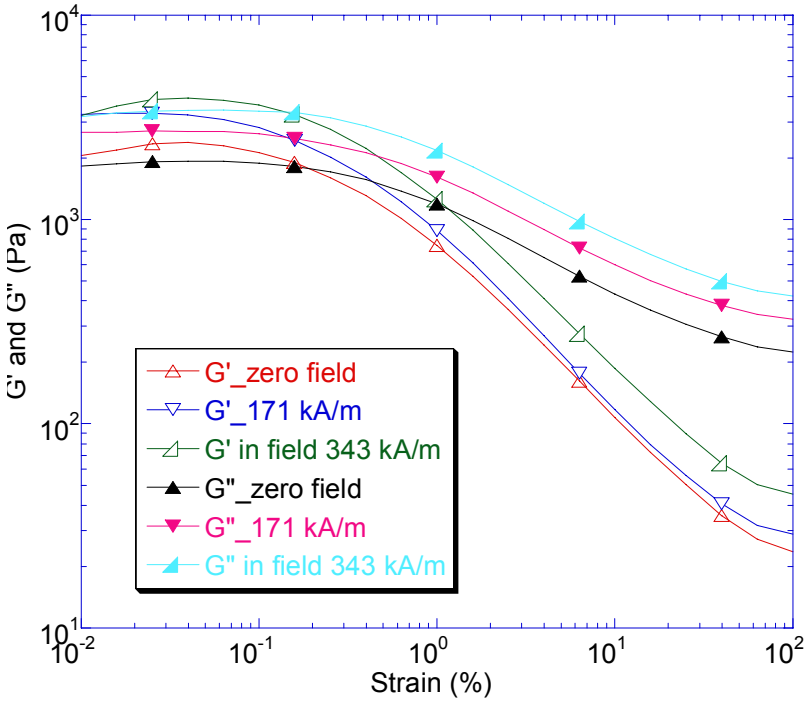

Fig. 3.43 Strain sweeps for 2vol% MWCNT/ep dispersions under various magnetic fields.

Table 3.14 G' and G" at the strain of 1% for MWCNT/ep dispersions under various magnetic fields.

Composition	Magnetic field strength (kA/m)	Magnetic flux density (Tesla)	G' at strain of 1% (Pa)	G" at strain of 1% (Pa)
0.67vol%MWCNT/ep	0	0	7.98	156
0.67vol%MWCNT/ep	343	0.215	13.9	177
2vol%MWCNT/ep	0	0	748	1190
2vol%MWCNT/ep	171	0.215	884	1610
2vol%MWCNT/ep	343	0.431	1260	2170

Table 3.15 Critical strain γ_c and G at γ_c during strain sweeps for 2vol% MWCNT/ep dispersions under various magnetic fields.

Composition	Magnetic field strength (kA/m)	Magnetic flux density(Tesla)	Critical strain γ_c (%)	G at γ_c (Pa)
2vol%MWCNT/ep	0	0	0.194	1756
2vol%MWCNT/ep	171	0.215	0.1487	2512
2vol%MWCNT/ep	343	0.431	0.1398	3357

3.4.2 Frequency Sweeps of MWCNT/ep Dispersions

The frequency sweeps for 0.67vol% and 2vol% MWCNT/ep dispersions are shown in Fig. 3.44 and Fig. 3.45, respectively. Similar to the strain sweeps, no G'-G" crossover is for 0.7vol% and one G'-G" crossover is observed for 2vol%. The frequency at G'-G" crossover in an applied field is higher than that in a zero field as shown in Table 3.16.

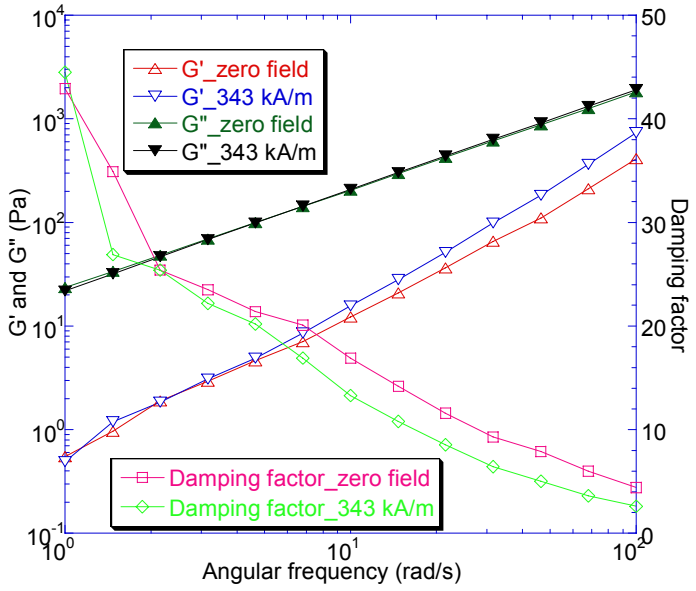

Fig. 3.44 Frequency sweeps for 0.67vol% MWCNT/ep dispersions under various magnetic fields.

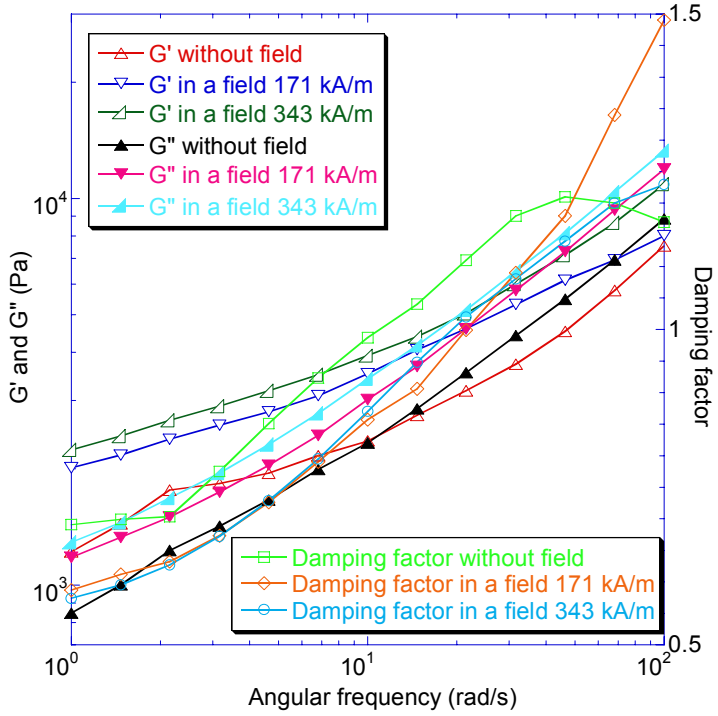

Fig. 3.45 Frequency sweeps for 2vol% MWCNT/ep dispersions under various magnetic fields.

Table 3.16 Angular frequency ω at G'-G" crossover for MWCNT/ep dispersions under different magnetic fields.

Composition	Magnetic field strength (kA/m)	Magnetic flux density (Tesla)	ω at G'-G" crossover (rad/s)
2vol%MWCNT/ep	0	0	10.76
2vol%MWCNT/ep	171	0.215	21.71
2vol%MWCNT/ep	343	0.431	18.94

3.4.3 Steady Shear Tests of MWCNT/ep Dispersions

The flow curves of 0.67vol% MWCNT/ep shown in Fig. 3.46 indicate all curves under various magnetic fields are roughly the same. Fig. 3.47 shows the flow curves of 2vol% MWCNT/ep and the shear stress increases slightly with increasing magnetic field at the same shear rate.

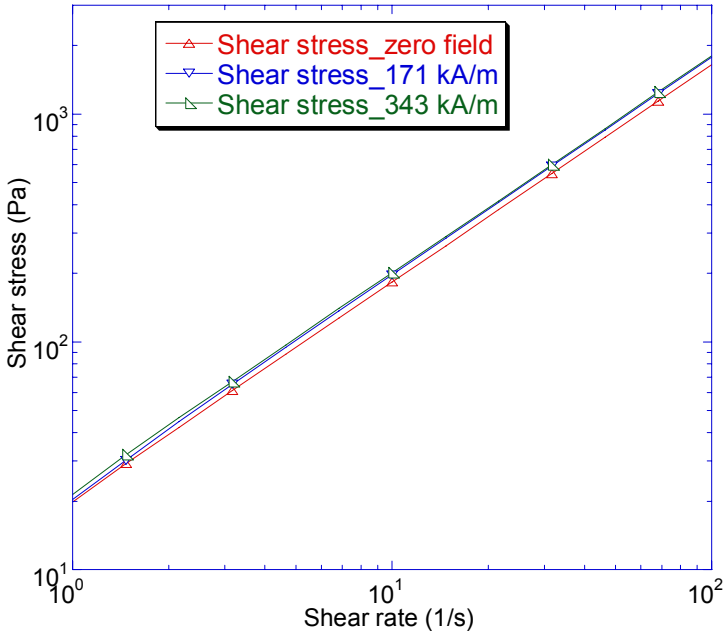

Fig. 3.46 Flow curves for 0.67vol% MWCNT/ep under various magnetic fields.

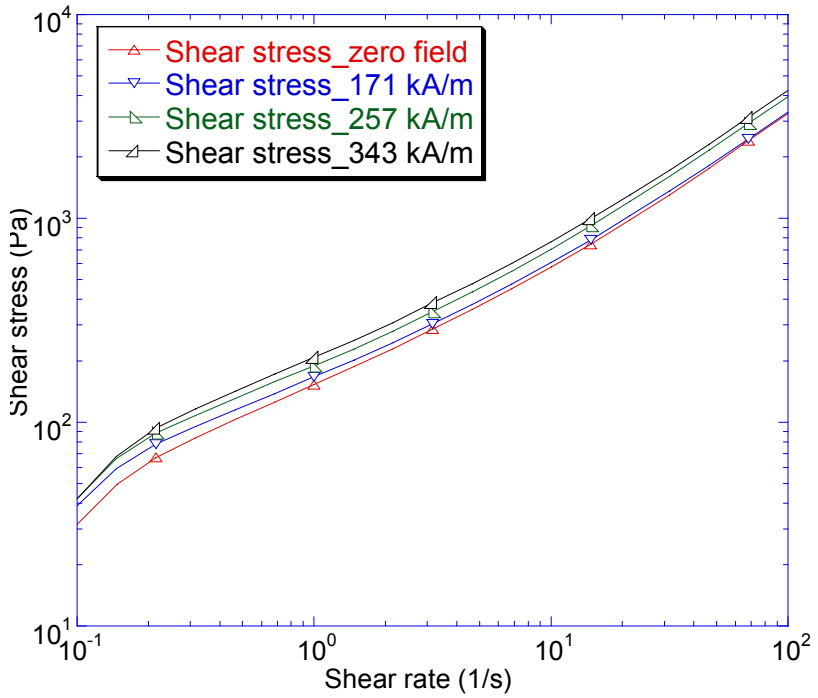

Fig. 3.47 Flow curves for 2vol% MWCNT/ep under various magnetic fields.

The yield stresses obtained from the flow curves are listed in Table 3.17. For 0.67vol%MWCNT/ep, the yield stress remains approximately the same under different fields. At a concentration of 2vol%, the yield stress increases with increasing magnetic field.

Table3.17 Yield stress for MWCNT/ep dispersions under various magnetic fields.

Sample	Magnetic field strength (kA/m)	Magnetic flux density (Tesla)	Yield stress (Pa)
0.67vol%MWCNT/ep	0	0	2.19
0.67vol%MWCNT/ep	171	0.215	0.997
0.67vol%MWCNT/ep	343	0.431	2.05
2vol%MWCNT/ep	0	0	21.9
2vol%MWCNT/ep	171	0.215	30.78
2vol%MWCNT/ep	257	0.323	33
2vol%MWCNT/ep	343	0.431	29.88

Fig. 3.48 shows the normalized G', G" and η* for 0.67vol% MWCNT/ep and 2vol% MWCNT/ep during magneto sweeps. 0.67vol% MWCNT/ep exhibits larger percent increase in G' and G" than 2vol% MWCNT/ep. The relative increases in complex viscosity for both concentrations are roughly the same.

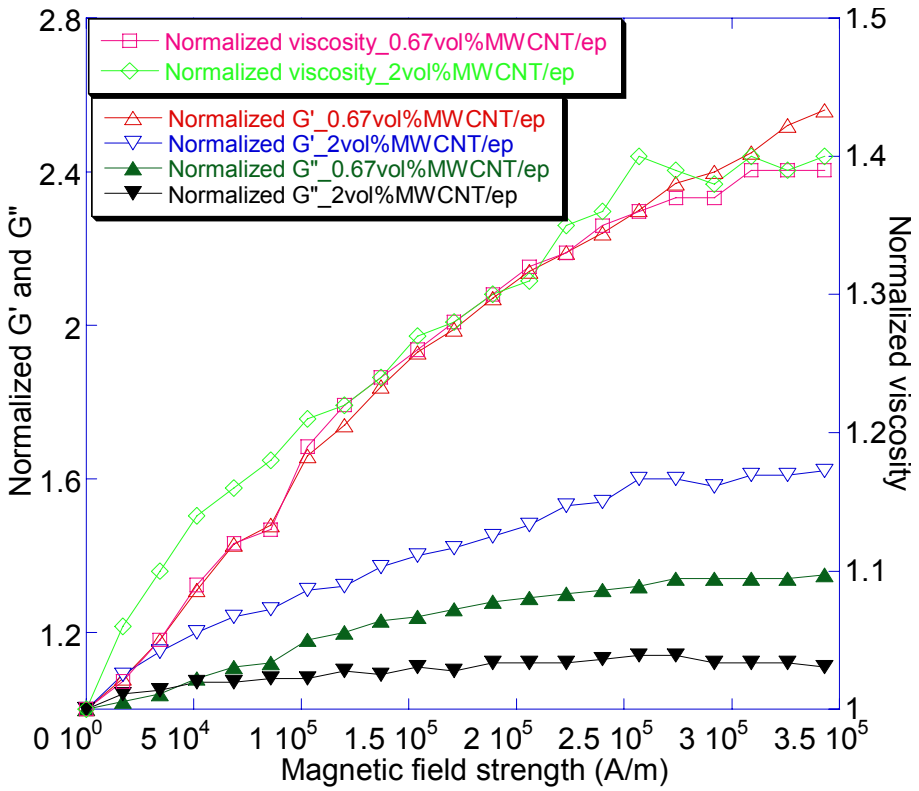

Fig. 3.48 Normalized G', G" and η* for 0.67vol% MWCNT/ep and 2vol% MWCNT/ep during magneto sweeps.

CHAPTER 4

CONCLUSIONS

The magnetorheological behaviors of SWCNT/mo, SWCNT/ep, MWCNT/mo and MWCNT/ep dispersions with different concentrations were investigated. Increasing the magnetic field increased G', G", η^* and τ_y mainly due to the increasing degree of the alignment of nanotubes along the magnetic field direction in a stronger magnetic field. The effect of alignment depended strongly on the viscosities of the dispersions and nanotube concentrations. SWCNT/mo dispersions exhibited a much stronger response to an applied magnetic field than SWCNT/ep, MWCNT/mo and MWCNT/ep dispersions mainly due to the lowest viscosities of SWCNT/mo dispersions.

2.5vol%SWCNT/mo showed the largest degree of alignment. The critical strain for 6.41vol% SWCNT/mo increased with increasing magnetic field. For SWCNT/mo dispersions, increasing the magnetic field resulted in a weaker frequency dependence of the G' and G", delayed the onset of non-Newtonian behavior and the transition from solid to liquid state and increased the elastic properties. The G'-G" crossover frequency increased with increasing SWCNT concentration in the same field and also increased with increasing field for the same composition. The G' and G" for SWCNT/mo scaled with ($H\varphi$) by a power law and the index of ($H\varphi$) for 2.5vol%SWCNT/mo was the highest. τ_y scaled with

magnetic flux density B by a power law. 2.5vol%SWCNT/mo exhibited the largest relative increase in G', G" and η^* while 6.41vol% SWCNT/mo showed the smallest increase in G', G" and η^* during magneto sweep, indicating the iron content is not the main reason for the observed increase in G', G" and η^* with increasing magnetic field. A flocculated system of 6.41 vol% SWCNT/mo behaved like a gel and restricted the alignment of the nanotubes.

For MWCNT/mo dispersions, the critical strain decreased with increasing magnetic field for 1.5 and 2.53vol%MWCNT/mo dispersions. one G'-G" crossover was evident for 1.5vol% and 2.53vol% MWCNT/mo dispersions and the crossover frequency decreased with increasing nanotube concentration in the same field and also decreased with increasing field strength for MWCNT/mo dispersions. The percent increase in G', G" and η^* during the magneto sweeps decreased with increasing MWCNT concentration and 0.5vol% MWCNT/mo exhibited the largest percent increase in G', G" and η^* while 2.53vol% MWCNT/mo showed the lowest relative increase in G', G" and η^*. The shear thinning behavior of SWCNT/mo and MWCNT/mo dispersions followed the Ostwald-de Waele or power law.

A G'-G" crossover was observed for the strain sweeps and frequency sweeps for the 2vol% MWCNT/ep dispersions. The critical strain decreased with increasing magnetic field. The frequency at G'-G" crossover under an applied field was higher than that without an applied field.

REFERENCE LIST

[1] Iijima S, Helical microtubules of graphitic carbon. Nature 1991; 354-356.

[2] Thostenson, ET, Ren Z, Chou TW. Advances in the science and technology of carbon nanotubes and their composites: A review. Composites Science and Technology 2001; 61:1899-1912.

[3] Dresselhaus MS, Dresselhaus G, Eklund PC. Science of fullerenes and carbon nanotubes 1996; Academic Press, San Diego.

[4] Tang W, Santare MH, Advani SG. Melt processing and mechanical property characterization of multi-walled carbon nanotube/high density polyethylene (MWCNT/HDPE) composite films. Carbon 2003; 41:2779-2785.

[5] Treacy MMJ, Ebbesen TW, Gibson TM. Exceptionally high Young's modulus observed for individual carbon nanotubes. Nature 1996; 381: 680-687.

[6] Wong EW, Sheehan PE, Lieber CM. Nanobeam mechanics: Elasticity, strength, and toughness of nanorods and nanotubes. Science 1997;277:1971-1975.

[7] Salvetat JP, Briggs GAD, Bonard JM, Bacsa RR, Kulik AJ, Stöckli T, Burnham NA, Forró L. Elastic and shear moduli of single-walled carbon nanotube ropes. Physical Review Letters 1999; 82: 944–947.

[8] Walters DA, Ericson LM, Casavant MJ, Liu J, Colbert DT, Smith KA, Smalley RE. Elastic strain of freely suspended single-wall carbon nanotube ropes. Applied Physics Letters 1999;74: 25, 3803-3805.

[9] Yu MF, Lourie O, Dyer M, Moloni K, Kelly T. Strength and breaking mechanism of multi-walled carbon nanotubes under tensile load. Science 2000; 287: 637-640.

[10] Yu MF, Files BS, Arepalli S, Ruoff RS. Tensile loading of ropes of single wall carbon nanotubes and their mechanical properties. Physical Review Letters 2000; 84:24, 5552-5555.

[11] Sandler JKW, Kirk JE, Kinloch IA, Shaffer MSP, Windle AH. Ultra-low electrical percolation threshold in carbon-nanotube-epoxy composites. Polymer 2003; 44: 5893-5899.

[12] Biercuk MJ, Llaguno MC, Radosavljevic M, Hyun JK, Johnson AT, Fischer JE. Carbon nanotube composites for thermal management. Applied Physics Letters 2002;80:15, 2767-2769.

[13] Gong X, Liu J, Baskaran S, Voise RD, Young JS. Surfactant-assisted processing of carbon nanotube/polymer composites. Chemistry of Materials 2000; 12: 4, 1049-1052.

[14] Gojny FH, Nastalczyk J, Roslaniec Z, Schulte K. Surface modified multi-walled carbon nanotubes in CNT/epoxy-composites. Chemical Physics Letters 2003; 370: 820-824.

[15] Ajayan PM, Stephen O, Colliex C, Trauth D, Science 1994; 265:1212.

[16] Jin L, Bower C, Zhou O. Applied Physics Letters 1998; 73:9,1197-1199.

[17] Thostenson ET, Chou TW. Aligned multi-walled carbon nanotube-reinforced composites: processing and mechanical characterization. Journal of Physics D: Applied Physics 2002;35: L77-L80.

[18] Ramirez AP, Haddon RC, Zhou O, Fleming RM, Zhang J, McClure SM, Smalley RE. Magnetic susceptibility of molecular carbon: Nanotubes and fullerite. Science 1994; 265:5168, 84-86.

[19] Lu JP. Novel magnetic properties of carbon nanotubes. Physical Review Letters 1995;74:7,1123-1126.

[20] Wang X K, Lin X W, Dravid VP, Ketterson JB, Chang RPH, Growth and characterization of buckybundles. Applied Physics Letters 1993; 62:16, 1881-1883.

[21] Fujiwara M, Fukui M, TanimotoY. Magnetic orientation of benzophenone crystals in fields up to 80.0 KOe. Journal of Physical Chemistry B 1999;103: 2627-2630.

[22] Fujiwara M, Oki E, Hamada M, Tanimoto Y, Mukouda I, Shimomura Y, Magnetic orientation and magnetic properties of a single carbon nanotube, Journal of Physical Chemistry A 2001;105:18, 4383 -4386.

[23] Walters DA, Casavant MJ, Qin XC, Huffman CB, Boul PJ, Ericson LM, Haroz EH, O'Connell MJ, Smith K, Colbert DT, Smalley RE. In-plane-aligned membranes of carbon nanotubes. Chemical Physics Letters 2001; 338:14-20.

[24] Casavant MJ, Walters DA, Schmidt JJ, Smalley RE. Neat macroscopic membranes of aligned carbon nanotubes. Journal of Applied Physics 2003; 94: 4, 2153-2156.

[25] Kimura T, Ago H, Tobita M, Ohshima S, Kyotani M, Yumura. Polymer composites of carbon nanotubes aligned by a magnetic field. Advanced Materials 2002;14:19,1380-1383.

[26] Gupta R K. Polymer and composite rheology. 2000, New York, Marcel Dekker, Inc.

[27] Einstein A. Investigation on the theory of the Brownian movement. Dover 1956, New York, 36-54.

[28] Shaffer MSP, Fan X, Windle AH. Analogies between polymer solutions and carbon nanotube dispersions. Micromolecules 1999; 32:6864-6866.

[29] Kinloch IA, Roberts SA, Windle AH. A rheological study of concentrated aqueous nanotube dispersions. Polymer 2002; 43: 7483-7491.

[30] Pötschke P, Fornes T D, Paul DR. Rheological behavior of multiwalled carbon nanotube/polycarbonate composites. Polymer 2002; 43: 3247-3255.

[31] Ginder JM. Behavior of magnetorheological fluids. MRS bulletin August 1998; 26-29.

[32] Rabinow J. AIEE Trans 1948; 67:1308.

[33] Ginder JM, Davis LC, Elie LD. Rheology of magnetorheological fluids: Models and measurements. International Journal of Modern Physics B 1996;10: 23-24, 3293-3303.

[34] Timko M, Zentko A, Zentkova M, Koneracka M, Kellnerova V, Zentkova A, Stepan M, Barbora J. Magnetorheological properties of some ferrofluids. IEEE Transactions on Magnetics 1994; 30: 2, 1117 – 1119.

[35] Wollny K, Lauger J, Huck S. Magneto sweep-a new method for characterizing the viscoelastic properties of magneto-rheological fluids. Applied Rheology 2002;12:1, 25-31.

[36] Läuger J, Huck S, Wollny K. Magneto Sweep: A method to characterize magneto rheological fluids. Physica Messtechnik GmbH,Stuttgart/Germany

[37] Claracq J, Sarrazin J, Montfort JP, Viscoelastic properties of magnetorheological fluids. Rheol Acta 2004; 43: 38-49.

[38] McLeish TCB, Jordan T, Shaw MT. Viscoelastic response of electrorheological fluids. I. Frequency dependence. Journal of Rheology 1991; 35: 3, 427-448.

[39] Klingenberg DJ, Simulation of the dynamic oscillatory response of electrorheological suspensions: Demonstration of a relaxation mechanism. Journal of Rheology 1992; 37: 2,199-214.

[40] Macosko C W. Rheology: Principles, measurements, and applications. New York, Wiley-VCH 1993.

[41] Phule PP, Ginder J M. Synthesis and properties of novel magnetorheological fluids having improved stability and redispersibility. International Journal of Modern Physics B 1999;13:14, 2019-2027.

[42] Kitano T, Kataoka T, Nagatsuka Y. Shear flow rheological properties of vinylon- and glass-fiber reinforced polyethylene melts. Rheological Acta 1984; 23: 20-30.